Full characterization and calibration of a transfer standard monitor for atmospheric radon measurements

Roger Curcoll[1], Claudia Grossi[1,2], Stefan Röttger[3], Arturo Vargas[1]

[1]Institut de Tècniques Energètiques (INTE), Universitat Politècnica de Catalunya, Barcelona, Spain
[2]Department of Physics, Universitat Politècnica de Catalunya, Barcelona, Spain
[3]Physikalisch-Technische Bundesanstalt, 38116 Braunschweig, Germany

Correspondence to: Roger Curcoll (roger.curcoll@upc.edu)

Abstract.

In this work a full characterization of the new user-friendly version of the Atmospheric Radon MONitor (ARMON), used to measure very low activity concentrations of the radioactive radon gas in the outdoor atmosphere, is carried out. The ARMON is based on the electrostatic collection of $^{218}Po^+$ ions on a semiconductor detector surface. A main advantage of this instrument is offering high resolution alpha energy spectra which will allow to separate radon progeny (^{210}Po, ^{218}Po and ^{214}Po). The monitor feature may also allow measurements of thoron (^{220}Rn) by collection of $^{216}Po^+$, although the instrument is not calibrated for this gas.

In this work the physical principle, the hardware configuration and the software development of the automatic and remotely controlled ARMON, conceived and constructed within the MAR^{2}EA and the traceRadon projects, are described. The monitor efficiency and its linearity over a wide span of radon concentration activities has been here evaluated and tested using theoretical as well as experimental approaches. Finally, a complete budget analysis of the total uncertainty of the monitor was also achieved.

Results from the application of a simplified theoretical approach shows a detection efficiency for $^{218}Po^+$ of about 0.0075 (Bq m^{-3})$^{-1}$ s^{-1}. The experimental approach, consisting of exposing the ARMON at controlled radon concentrations between few hundreds to few thousands of Bq m^{-3}, gives a detection efficiency for $^{218}Po^+$ of 0.0057 ± 0.0002 (Bq m^{-3}) s^{-1}. This last value and its independence from the radon levels was also confirmed thanks to a new calibration method which allows, using low emanation sources, to obtain controlled radon levels of few tens of Bq m^{-3}.

The total uncertainty of the ARMON detection efficiency obtained for hourly radon concentration above 5 Bq m^{-3} was lower than 10 % (*k*=1). The characteristics limits of the ARMON were also calculated, being dependent on the presence of thoron in the sampled air, and a value of 0.132 Bq m^{-3} was estimated in thoron absence. At a typical thoron concentration at atmospheric sites of 0.017 min^{-1}, the detection limit was calculated to be 0.3 Bq m^{-3}, but can be reduced if using a delay volume, obtaining a decision threshold of 0.0045 Bq m^{-3}. Current results may allow to confirm that the ARMON is suitable to measure low-level radon activity concentration (1 Bq m^{-3} - 100 Bq m^{-3}) and to be used as transfer standard to calibrate secondary atmospheric radon monitors.

1 Introduction

^{222}Rn is a radioactive noble gas naturally generated from Radium (^{226}Ra) within the primordial Uranium-238 (^{238}U) decay chain (Nazaroff and Nero, 1988). Its exhalation from soils depends mainly on the uranium content, soil properties as porosity or bulk density, and soil moisture (Conen and Robertson, 2002). The global ^{222}Rn source into the atmosphere is mainly

40 restricted to land surfaces (Szegvary et al., 2009; Karstens et al., 2015), with the ^{222}Rn flux from water surfaces considered negligible for most applications (Schery and Huang, 2004). Radon has a half-life of about 3.82 days and, due to the fact that does not have any other significant atmospheric sink rather than its radioactive decay, has been largely used in the last decades as a tracer for atmospheric studies. ^{222}Rn has been used to understand atmospheric processes such as the dynamics of the boundary layer (Chambers et al., 2011; Pal et al., 2015; Vargas et al., 2015), to improve inverse transport models (Hirao et al.,

45 2010), to assess the accuracy of chemical transport models (Jacob and Prather, 1990; Arnold et al., 2010; Chambers et al., 2019), or to study atmospheric transport and mixing processes within the planetary boundary layer (Zahorowski et al., 2004; Galmarini, 2006; Baskaran, 2011, 2016; Williams et al., 2016). When measured together with another gas (e.g. air pollutants or greenhouse gases such as carbon dioxide or methane), it can be also used to detect sources and to indirectly quantify fluxes of that gas. The Radon Tracer Method (RTM) (Levin et al., 1999) is one of the methodologies used to indirectly determine

50 regional and nocturnal fluxes of greenhouse gases and air pollutants (Vogel et al., 2012; Wada et al., 2013; Levin et al., 2021). In addition, if RTM is used together with back trajectories analyses, it will allow a better quantification of the different local versus regional contributions and an estimation of the effective radon flux seen by the station under study (Grossi et al., 2018).

For its utility, ^{222}Rn measurements are so far not mandatory but recommended at the atmospheric stations of the Integrated Carbon Observation System network (ICOS RI, 2020). Atmospheric radon activity concentrations are usually ranging between

55 few hundreds of mBq m^{-3} and tens of Bq m^{-3}, depending if the measurements are carried on at coastal or continental sites, respectively (Chambers et al., 2016; Grossi et al., 2016). Thus, high precision radon measurements are required for atmospheric applications.

Available commercial radon monitors, usually used in the radiation protection field or for geophysics research goals, are so far not suitable for high quality atmospheric measurements too (Radulescu et al., 2022). In the last years three research entities

60 have designed and developed high sensitive ^{222}Rn or ^{222}Rn progeny monitors which are currently running at different European atmospheric stations: i) the Heidelberg monitor, developed at the Institute of Environmental Physics of the Heidelberg University (Schmidt et al., 1996; Levin et al., 2002), determines the atmospheric ^{222}Rn activity concentration using the measured ^{214}Po daughter activity with a static filter method and assuming a constant equilibrium factor between radon and its short lived progeny in air. (Schmithüsen et al., 2017); ii) the monitor from the Australian Nuclear Science and Technology

65 Organisation (ANSTO), which determines the atmospheric ^{222}Rn activity concentration using dual-flow-loop two-filter method (Whittlestone and Zahorowski, 1998; Zahorowski et al., 2004); iii) the Atmospheric Radon MONitor (ARMON), designed and built at the Institute of Energy Technologies (INTE) of the Universitat Politècnica de Catalunya (UPC), which is based on alpha spectrometry from the positive ions of ^{218}Po electrostatically collected on a Passivated Implanted Planar Silicon (PIPS) detector surface (Grossi et al., 2012; Vargas et al., 2004, 2015). Several monitors of this last type have been displaced at

70 atmospheric Spanish stations for atmospheric research studies (Grossi, 2012; Hernández-Ceballos et al., 2015; Vargas et al., 2015; Grossi et al., 2018; Gutiérrez-Álvarez et al., 2019). The response of the ARMON under different field conditions was also compared with the ones from other previously cited research instruments in the south of Paris in 2016 (Grossi et al., 2020).

In the framework of the Catalan MAR^{2}EA project (High Efficiency monitor of atmospheric radon concentration for radioprotection and environmental applications, Llavor program, 2020-2021) and of the Working Package 1 (WP1) of the

75 European traceRadon project (Röttger et al., 2021), an improved ARMON prototype was developed (here labelled as ARMON v2). The main objective of the traceRadon project was the development of a metrological infrastructure to ensure traceability of low levels radon measurements. Specifically, the WP1 aimed to develop traceable methods, according to IEC 61577, for the measurement of outdoor low-level radon activity concentrations in the range of 1 Bq m^{-3} to 100 Bq m^{-3}, with uncertainties lower than 10 % (k=1), to be used in climate and radiation protection networks. Within this WP1, the INTE-UPC group was

80 in charge to design and build a mobile and user-friendly transfer standard instrument useful to calibrate radon monitors running

at atmospheric and radiological stations. This new user-friendly monitor is an improved version of the previous ARMON, mainly in regard to its robustness, portability, sensitivity, setting and automatic control.

In the present manuscript the design and setup of the ARMON v2 are described in detail together with the theoretical and experimental methodologies applied to evaluate the detection efficiency of the monitor. The total uncertainty of the ARMON v2 detection efficiency was also calculated considering the different parameters and variables that could influence it such as the statistic number of counts of each alpha spectrum measured by the ARMON v2, the effect of the water content of the sampled air, the STP (Standard Temperature and Pressure) correction, the monitor background, etc.

The ARMON v2 was calibrated at the INTE-UPC radon chamber using reference radon concentrations between few hundred Bq m^{-3} and few thousand Bq m^{-3}. In order to check if the detection efficiency obtained thanks to the INTE-UPC exposures was also confirmed for very low radon activities concentrations (tens of Bq m^{-3}), an independent experiment was carried out at the Physikalisch-Technische Bundesanstalt (PTB) facility, using new low radon emanation sources and methods also generated within the WP1 of the traceRadon project.

The ARMON v2 presented in this paper, thanks to its sensitivity and robustness, has the potential to help in the improvement of the sources, transport, and fate of ^{222}Rn in the environment. The full characterization of this instrument and its uncertainty budget may be useful to support the development of accurate atmospheric studies and to enhance the capabilities of the Radon Tracer Method for estimating GHG fluxes.

2 ARMON description

2.1 Physical principles of the ARMON v2

The physical principle of operation of the ARMON is based on the collection of the positive ^{218}Po charged ions, due to the alpha decay of the ^{222}Rn within the detection volume, on the surface of a semiconductor detector. This methodology is well known and has been used in the past by other researchers (Grossi et al., 2012; Hopke, 1989; Tositti et al., 2002; WADA et al., 2010). ^{218}Po$^+$ ions, generated within a known volume, are found to be in the form of singly charged positive ions the 88 % of the time, while the neutral ions occur the remaining 12 % of the time (Goldstein and Hopke, 1985). ^{218}Po$^+$ can be due to the stripping of orbital electrons by the departing α particle or by the recoil motion. When a high electric potential is applied to the internal surface of the detection volume and the detector itself is maintained at 0 V, an Electrostatic Field (EF) is generated inside the volume, causing the charged ^{218}Po$^+$ ions to be collected at the detector surface within short time.

In the case of the ARMON, a Passivated Implanted Planar Silicon (PIPS) detector is used. A preamplifier and an amplifier are then used to amplify and shape the electric signal coming from the detector to a Gaussian shape in order to be read by a multichannel analyser (MCA), that transforms it into counts for specific energy bins. The spectra generated are then analysed with the software MAESTRO (Multichannel Analyzer Emulation Software, ORTEC). A typical one-hour spectrum from atmospheric radon in air obtained with the ARMON v2 is shown in the Appendix A (Fig. A1).

Using this previous methodology, the ^{218}Po counts (with an α decay energy of about 6.0 MeV) can be separated in the spectrum from other ^{222}Rn progeny isotopes such as the ^{214}Po (α decay energy of about 7.7 MeV) and the ^{210}Po (α decay energy of about 5.3 MeV). Using the same principle, the ARMON v2 is also able to measure ^{220}Rn by detection of its progeny ^{216}Po (α decay energy of about 6.8 MeV) and ^{212}Po (8.78 MeV). However, in the present manuscript the full characterization of the instrument was only carried out for radon measurements due to the lack of a metrology chain for low-level thoron measurements. In this regard, it is needed to be clarified that if ^{220}Rn (thoron) is also present within the sampled air, ^{212}Bi particles, due to its decay chain, are also formed through β-decay of ^{212}Pb. The 36 % of this ^{212}Bi, α-decays to ^{208}Tl at a similar energy than ^{218}Po (6.05 MeV) and affects the net counts of ^{218}Po and thus the uncertainty of the final radon measurements, as explained in Grossi et al., 2012 and Vargas et al., 2015. The other 64 % of the ^{212}Bi particles β-decay to ^{212}Po (t$_{1/2}$ = 3.0 10^{-7} s), which α-decays at

8.78 MeV to the stable nuclide ^{208}Pb. Thanks to the high energy resolution of the ARMON spectra, the decay of the ^{212}Po ions can be registered, separated and counted. Therefore, the ^{212}Bi counts can be estimated by multiplying the factor 36/64 to the ^{212}Po counts, and its contribution may be subtracted from the gross ^{218}Po counting. The radon concentration is thus calculated for each spectrum of real time length t (in seconds), from the Eq. (1):

$$C_{Rn} = \left[\frac{nc_{Po218}}{t} - \left(\frac{nc_{Po212}}{t} \frac{36}{64} \right) \right] \frac{1}{\varepsilon} \quad (1)$$

Where nc_{Po218} is the number of counts detected within the ROI (region of interest) of ^{218}Po, nc_{Po212} is the number of counts detected within the ROI of ^{212}Po, t is the integration time of the spectrum, ε is the detection efficiency of the instrument, defined as detected ^{218}Po count rate per ^{222}Rn air concentration, and here expressed in counts per seconds (cps, s^{-1}) per Bq m^{-3}. It is also important to underline that charged ^{218}Po ions present within the detection volume may be neutralized due to the interaction with water vapour present in the sampled air via the formation of hydroxyl radicals OH (Hopke, 1989). Therefore, water vapour particles must be kept as low as possible inside the detection volume in order to maximize the collection efficiency, and the response of the monitor under different water vapour content conditions must be corrected. Assuming a linear correction of the efficiency due to water vapour concentration (Hopke, 1989), the real efficiency of our monitor can be expressed by Eq. (2), where ε_0 is the efficiency in dry condition (0 ppmv of H$_2$O), b is the trend of the linear correction and $[H_2O]$ is the water vapour concentration.

$$\varepsilon = \varepsilon_0 - b[H_2O] \quad (2)$$

2.2 ARMON v2 set up: Hardware and Software

A schematic design of the ARMON v2 is shown in Fig. 1a. A photography of the external case is shown in Fig. 1b. Before entering the detection volume, the air, sampled with a pump, (blue line in Fig. 1a) passes through a 0.5 μm filter to prevent the entry of dust and aerosol attached ^{222}Rn progeny into the detection volume. Then the air enters into the detection volume which is made by a glass sphere inside silver-plated with a neck of 45 mm of inner diameter. The PIPS detector of 300 mm^2 active area (Mirion Technologies A300-17) is located on the upper part of the sphere, tangent to it and at the bottom of the neck. This last configuration was used to maximize the collection of the polonium by the EF as shown later and it was obtained using a solid Teflon stopper. A high voltage power supply (Glassman MJ15P1000) provides a potential of 10 kV between the PIPS detector (at 0 V) and the sphere walls to create the EF. The pulse pre-amplifier and amplifier (model: CR-10 from Pyramid Technical Consultants Inc.) is located outside the sphere to shape and to amplify the signal and to send it to the MCA (model: ORTEC EASY-MCA 2k). When the sampled air exits the detection volume, it passes through a series of sensors: a digital flow meter (SMC PFM710S-F019), a temperature meter (JUMO PT100) and a dew point meter (VAISALA DMT 143). The sensors are controlled by a datalogger (Advantech USB-4622-CE) connected to a laptop. All the hardware is installed inside a flight-case box of 128x50x50 cm^3, with the inlet and outlet air sampling connectors located on the backside of the case (Fig 1b). The different components of the instrument are placed on different trays and drawers in order to easily access them and make the necessary maintenance if needed. A drawing and photos of the monitor are shown in the Appendix A (Fig. A2). The inlet flow required for the monitor is of about 2 L min^{-1} of dried air.
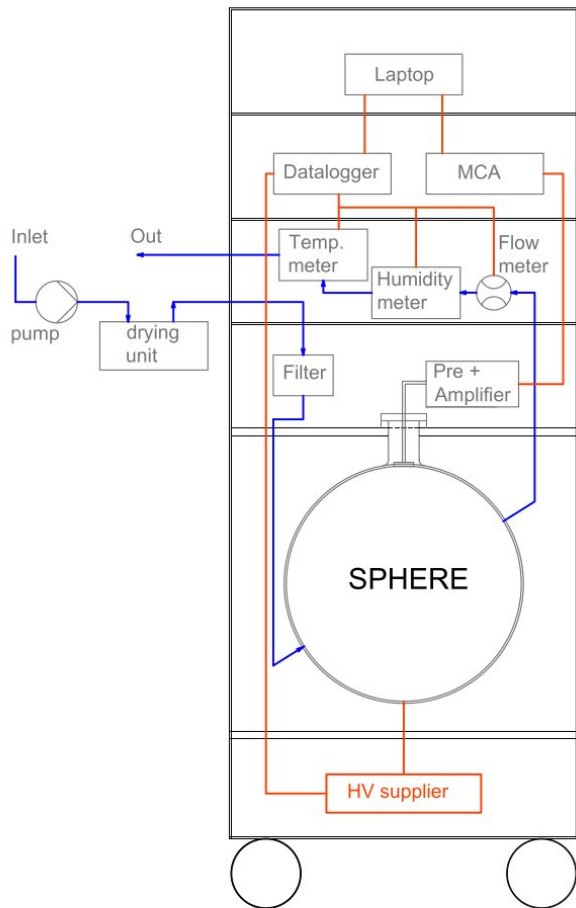
a)

b)

Figure 1. a): schematic design of the ARMON v2 with its main hardware's and their location. b): Image of the backside of the instrument.

A specific software named ARMON_LAB, built on LabVIEW® (Laboratory Virtual Instrument Engineering Workbench), was
160   developed in order to monitor and to control all the parameters and variables of the instrument with the help of the Advantech®
datalogger. The software is installed in the ARMON v2 laptop to give the user a full control of the monitor. The software
allows the visualization in real time of the different sensors' outputs (flow, humidity and temperature) and allows the control
of the high voltage applied to the detection volume. Ten minutes' averages of the different variables are automatically saved
in daily files. In parallel, the spectra obtained by the MCA are automatically and regularly saved using the Maestro software
165   script (ORTEC, 2012). After each measurement (usually working on hourly base for atmospheric stations requirements but it
can be easily modified) the ARMON_LAB software calls an R script which uses the information from the Maestro and the
output from the environmental sensors to calculate the radon concentration. Real-time as well as past radon concentrations
data can be visualized within the ARMON_LAB interface. Two screenshots of the software are shown in the Appendix A
(Fig. A3). The laptop can be connected to internet whether by Wi-Fi or by an ethernet wire and, once installed, the instrument
170   can be fully remotely controlled. A flow chart of the data of the ARMON v2 monitor is shown in the Appendix A (Fig. A4).

2.3 ARMON v2 detection efficiency

2. 3.1 Theoretical approach

In order to calculate the radon concentration measured by the ARMON v2 with Eq. 1, the total efficiency (ε) of the instrument needs to be known with the lowest uncertainty achievable. First of all, the order of magnitude of this efficiency was evaluated using a simplified theoretical approach. The theoretical detection efficiency of the ARMON v2, ε_t, can mainly be factorized in two terms: the geometric contribution (ε_g) due to the geometry of the detector surface and corona and the collection efficiency (ε_c) that depends on the efficiency of the collection of the $^{218}Po^+$ on the detector active surface. The two contribution are expressed in Eq. 3:

$$\varepsilon_t = \varepsilon_g \cdot \varepsilon_c \qquad (3)$$

The analysis of these two factors allowed to optimize them during the building of the monitor. As commented in Section 2.1, the maximum possible percentage of positive charged ^{218}Po ions collected over the detector surface is of 88 % (Hopke, 1989) ($p_{218_{Po^+}}$). However, both the active surface of the PIPS detector and the not active surface (the corona) are at the same potential (0 V), so when the ions reach the detector, they will be distributed over the entire surface, both on the active part and on the non-active one. Luckily, this distribution is not spatially homogenous and it will depend on the symmetry and geometry of the generated EF as it will be shown here. Furthermore, of those ions collected at the active surface (p_{Active}), only about 50 % will be emitting alpha particles on the plane including the detector and therefore counted ($p_{Detected}$), as those emitted in the opposite direction away from the detector cannot be counted. The number of ions per second that are formed in the sphere for a radon concentration in air of 1 Bq m^{-3} are calculated by multiplying the formed ions $p_{218_{Po^+}}$ by the sampled air volume V (0.02 m^3) and then multiplied by the percent of ions arriving on the detector surface and emitting in the detector plane. The resulting ε_g in s^{-1} per Bq^1 m^{-3} is calculated according Eq. 4.

$$\varepsilon_g = V\, p_{218_{Po^+}} \cdot p_{Active} \cdot p_{Detected} \qquad (4)$$

In order to understand and thus to maximize the collection of the polonium ions on the detector surface, the software COMSOL Multiphysics (COMSOL, 2015) was used to simulate the shape of the EF generated within the ARMON v2 detection volume when different kV of electric potential (V) were applied to the sphere wall. The COMSOL is based on the solving of equations by finite element analysis. The output of the COMSOL simulation, with the value of the simulated electrostatic field at each spatial grid of the ARMON v2 detection volume, was then used to calculate the drift velocity, the collection trajectories, and the travelling time of 10000 polonium fictitious ions, which were initially randomly spaced within the volume. The instantaneous drift velocity for each particle i inside the detection volume depends on the mobility (μ) of the $^{218}Po^+$ ions and the EF at its position as reported in Eq. 5:

$$v_i = \mu \vec{E_i} \qquad (5)$$

The mobility of the $^{218}Po^+$ ions in air is known to be between 1 cm^2 (V s)$^{-1}$ and 6 cm^2 (V s)$^{-1}$ (Nazaroff and Nero, 1988; Pugliese et al., 2000). A mobility of 3 cm^2 (V s)$^{-1}$ was recently reported by Symour (2017) for a similar study and was also used in the present study. Trajectories were calculated using time steps of 10 μs. The arriving position of the simulated ions on the detector surface were used to estimate the percentage of polonium ions collected on the active area (2.99 cm^2) and on the not active area (3.44 cm^2) of the detector.

The percentage of polonium ions arriving on the detector's surface was calculated taking into account both the radioactive decay ($T_{1/2}$ = 184.3 s.) and the neutralization due to their recombination with OH$^-$ ions or small positive air ions (Dankelmann et al., 2001). In this regard, Hopke (1989) found that this recombination depends on the water volume concentration and that the interval time τ_{H_2O}, for ^{218}Po recombination in an electrostatic chamber had a value of 0.879 [H$_2$O]$^{-1/2}$, being [H2O] the

water vapor concentration in parts per million (ppm). From the calculated travelling time, equal to the ratio between the trajectory of each particle to reach the detector and its drift velocity, the effect of the recombination with water particles was calculated as Eq. 6:

$$N = N_o e^{-\log(2)\, t / (0.879\, [\text{H2O}]^{-1/2})} \qquad (6)$$

where N are the particles that has not been recombined within the travelling time t, N_o is the initial number of particles and $0.879\,[\text{H2O}]^{-1/2}$ is the interval time of recombination with H_2O for $^{218}Po^+$ ions. Finally, the theoretical collection efficiency ε_c will be calculated as N/N_o.

The theoretical efficiency ε_t obtained from Eq. 3 has been calculated under the hypothesos of ideal conditions. However, the real geometry of the generated EF may not be so regular due to: i) the difficulty of positioning the PIPS surface tangent to the sphere; ii) inhomogeneity present in the layer of the cover conductive material of the internal wall of the sphere; iii) uncertainty in the determination of the potential V applied to the sphere, and iv) the spherical shape and exact measure of the detection volume. Thus, the real efficiency of the monitor could be lower than ε_t and it needs also to be evaluated experimentally.

2.3.2 Experimental approach

The experimental detection efficiency of the ARMON v2 was obtained by comparing the detected net counts of ^{218}Po measured with the instrument with a reference radon activity concentration C_{Ref} measured with a secondary standard reference instrument as it will be explained in the following lines.

The ARMON v2 was calibrated at the INTE-UPC STAR (System for Test Atmospheres with Radon) (Vargas et al., 2004) in October 2021. The INTE-UPC STAR is a chamber with a volume of 20 m^3 which allows to set-up and to continuously measure the radon activity concentration (range 200 Bq m^{-3} to 30 kBq m^{-3}), the temperature (range 10 ºC – 40 ºC) and the relative humidity (range 15 % - 95 %) (Vargas et al., 2004). The radon source inside the chamber consists of an enclosed Pylon Electronics containing 2100 kBq of ^{226}Ra. Stable radon concentration inside the chamber are reached by controlling the air flow through the enclosed source and the ventilation rate of the chamber. The second standard reference instrument of this facility is an Atmos monitor (Radonova), serial number 220030. The traceability of the measured magnitude in Bq m^{-3} is referred to the Swedish Radiation Safety Authority (Calibration certificate n. SSM2021-2989-4) with an expanded uncertainty (k=2) of 6.7 % for 1500 Bq m^{-3}.

During the experiments, the ARMON v2 detection efficiency was estimated in a range of radon concentrations between 0.5 kBq m^{-3} and 6.2 kBq m^{-3}. The ARMON v2 and the reference monitor were installed outside the STAR in parallel configuration. For each instrument, air coming from the radon chamber was passing through monitor and then returned to the chamber. A silica gel dryer was installed before the air was entering at the ARMON v2 to reduce the water concentration of the sampled air. The integration time of the ARMON v2 spectra was chosen to be 1 h, and hourly means from the ATMOS were selected from the 10 min. default integration time. Calibration experiments lasted three weeks. The average H_2O concentration inside the ARMON's detection volume during the efficiency experiments was of about 300 ppmv. The influence of the water vapour concentration on the efficiency was also evaluated at different radon concentrations within the range (635 – 5900) Bq m^{-3} and within the range (100 – 3000) ppmv H_2O, by using different levels of saturated silica gel as dryer.

2.4 Uncertainty analysis and characteristic limits of the ARMON v2

The radon activity concentration with the ARMON v2 is calculated, for each acquired spectrum, from Eq. 1 and its unit is Bq m^{-3}. In order to have comparable results with radon values from other stations or monitors, the concentration can be multiplied by a Standard Temperature and Pressure (STP) factor to standardize the concentration obtained to a referenced value of Temperature and Pressure of air. The STP factor, assuming an ideal gas behaviour, can be calculated by Eq. 7:

$$STP = C_T \, C_P = \frac{P_{ref}}{P} \frac{T}{T_{ref}} \quad (7)$$

Where C_T and C_P are the corrections for Temperature and Pressure respectively, with T and T_{ref} are the sampling temperature and the reference temperature respectively (in K), P and P_{ref} are the sampling pressure and the reference pressure respectively. Therefore, Eq. 1 can be expanded, taking into account both the corrected value of the monitor detection efficiency under different humidity conditions as expressed in Eq. 2 and the STP correction from Eq. 6 in the following Eq. 8:

$$C_{Rn} = \left[\frac{nc_{Po218}}{t} - \left(\frac{nc_{Po212}}{t} \frac{36}{64}\right)\right] \frac{1}{\varepsilon_0 - b\,[H_2O]} \frac{P_{ref}}{P} \frac{T}{T_{ref}} \qquad (8)$$

The uncertainty for the radon concentration measurement will calculated, in agreement with according Guide to the expression of uncertainty in the measurement (BIPM et al., 2008) as in Eq. 9:

$$u_{C_{Rn}}^2 = \sum_{i=1}^{n} \left(\frac{\partial C_{Rn}}{\partial x_i}\right)^2 u_{x_i}^2 \quad (9)$$

where x_i are the different variables from Eq. 8 taken in consideration for the propagation of the uncertainty.

Resolving the partial differential equations of Eq. 9 and using Eq. 8, the resulting equation is given in Eq. 10:

$$u_c^2(C_{Rn}) = \left(\frac{C_p\,C_T}{t\,\varepsilon}\right)^2 \left(u_{nc_{Po218}}\right)^2 + \left(-\frac{C_p\,C_T}{t\,\varepsilon}\frac{36}{64}\right)^2 \left(u_{nc_{Po212}}\right)^2 + \left(-\left[\frac{nc_{Po218}}{t} - \left(\frac{nc_{Po212}}{t}\frac{36}{64}\right)\right]\frac{C_p\,C_T}{(\varepsilon_0 - b\,[H_2O])^2}\right)^2 u_{\varepsilon_0}^2 +$$

$$\left(\left[\frac{nc_{Po218}}{t} - \left(\frac{nc_{Po212}}{t}\frac{36}{64}\right)\right]\frac{C_p\,C_T\,[H_2O]}{(\varepsilon_0 - b\,[H_2O])^2}\right)^2 u_b^2 + \left(\left[\frac{nc_{Po218}}{t} - \left(\frac{nc_{Po212}}{t}\frac{36}{64}\right)\right]\frac{C_p\,C_T\,b}{(\varepsilon_0 - b\,[H_2O])^2}\right)^2 u_{[H_2O]}^2 + \left(\left[\frac{nc_{Po218}}{t} -\right.\right.$$

$$\left.\left.\left(\frac{nc_{Po212}}{t}\frac{36}{64}\right)\right]\frac{C_T\,P_{ref}}{\varepsilon\,P^2}\right)^2 u_P^2 + \left(\left[\frac{nc_{Po218}}{t} - \left(\frac{nc_{Po212}}{t}\frac{36}{64}\right)\right]\frac{C_P}{\varepsilon\,T_{ref}}\right)^2 u_T^2 \quad (10)$$

Table 1 presents the different contributions to the total uncertainty of each radon measurement performed with the ARMON v2. In this example the average radon concentration, water vapour concentration, hourly [212]Po counting, atmospheric pressure and temperature from a 6 months intercomparison within the traceRadon project at Saclay Atmospheric Station (SAC) were selected as reference values to perform an estimation. Integration time for radon concentration measurement was of 1 h.

Quantity	Estimate	Type	Standard uncertainty	Probability distribution	v_i	Sensitivity coefficient	Contribution to the standard uncertainty
X_i	x_i		$u(x_i)$			c_i	$u_i(y)$
nc_{Po218}	nc_{Po218}	A	$\sqrt{nc_{Po218}}$	Normal	∞	$\dfrac{C_p\,C_T}{t\,F_{cal}}$	$c_i u(x_i)$
nc_{Po212}	nc_{Po212}	A	$\sqrt{nc_{Po212}}$	Normal	∞	$-\dfrac{C_p\,C_T}{t\,F_{cal}}\dfrac{36}{64}$	$c_i u(x_i)$
ε_0	0.0057 (Bq m⁻³)⁻¹ s⁻¹	B	0.01 (3%) [1]	Normal	∞	$-\left[\dfrac{nc_{Po218}}{t} - \left(\dfrac{nc_{Po212}}{t}\dfrac{36}{64}\right)\right]\dfrac{C_p\,C_T}{(\varepsilon_0 - b\,[H_2O])^2}$	$c_i u(x_i)$
b	5.4 10⁻⁷ (Bq m⁻³)⁻¹ s⁻¹ ppmv⁻¹	B	7.3 10⁻⁸ [2]	Normal	∞	$\left[\dfrac{nc_{Po218}}{t} - \left(\dfrac{nc_{Po212}}{t}\dfrac{36}{64}\right)\right]\dfrac{C_p\,C_T\,[H_2O]}{(\varepsilon_0 - b\,[H_2O])^2}$	$c_i u(x_i)$
$[H_2O]$	~250 ppmv	B	20% $[H_2O]$ + 1ppmv [3]	Normal	∞	$\left[\dfrac{nc_{Po218}}{t} - \left(\dfrac{nc_{Po212}}{t}\dfrac{36}{64}\right)\right]\dfrac{C_p\,C_T\,b}{(\varepsilon_0 - b\,[H_2O])^2}$	$c_i u(x_i)$
P	~1000 hPa	B	0.3 hPa [4]	Normal	∞	$-\left[\dfrac{nc_{Po218}}{t} - \left(\dfrac{nc_{Po212}}{t}\dfrac{36}{64}\right)\right]\dfrac{C_T\,P_{ref}}{\varepsilon\,P^2}$	$c_i u(x_i)$
T	~298 K	B	0.15 + 0.002*T [3]	Normal	∞	$\left[\dfrac{nc_{Po218}}{t} - \left(\dfrac{nc_{Po212}}{t}\dfrac{36}{64}\right)\right]\dfrac{C_P}{\varepsilon\,T_{ref}}$	$c_i u(x_i)$
C_{Rn}	Eq- (9)	Combined uncertainty (u) (Bq m⁻³)					$u = \sqrt{\sum u_i^2(y)}$

[1] Uncertainty from the calibration at INTE Radon Chamber
[2] Residual -Standard Error from correlation linear model according to calibration at INTE radon chamber.

[3]*From manufacturers documentation*
[4]*From ICOS Atmosphere Station specification, v2.0 (https://box.lsce.ipsl.fr/index.php/s/uvnKhrEinB2Adw9?path=%2FSpecifications)*

Table 1: Contributions of the different variable and/or parameters to the total uncertainty of a typical radon concentration measurement performed with the ARMON v2 at an atmospheric station.

Due to its long half-life, [210]Po activity will grow in the detector's surface. However, as the ARMON v2 is able to separate the energy of the alpha particles emitted by the different Polonium isotopes, even large activities of e [210]Po will not affect the counting of 218Po. Interference to the [218]Po counts are only due to [212]Bi as it was explained in Section 2.1. Therefore, the typical limits (threshold limit and detection limit) will depend on the presence of thoron within the sampled air.

According to the ISO 11929-4, the decision threshold of the activity ($a*$) can be calculated using Eq. 11:

$$a^* = k_{1-\alpha}\,\tilde{u}(0) = k_{1-\alpha}\sqrt{w^2\left(\frac{n_0}{t_g t_0} + \frac{n_0}{t_0^2}\right)} \quad (11)$$

where $k_{1-\alpha} = 1.645$, $\tilde{u}(0)$ is the standard uncertainty of the background, w is the calibration factor $(1/\varepsilon)$, n_0 is the number of counts of the background effect, and t_0 and t_g are the count times of the measurement and the background.

The detection limit, according to the same standard, can be calculated, with a 95 % confidence, as in in Eq. 12

$$a^{\#} = \frac{2\,a^* + (k^2\,w)/t_g}{1 - k^2\,u_{rel}^2(w)} \quad (12)$$

being the $u_{rel}(w)$ relative standard uncertainty of the estimated efficiency ε.

2.5 Evaluation of the linearity of the ARMON v2 detection efficiency for low radon concentrations

The linearity of the detection efficiency of the ARMON v2 was checked thanks to the availability of a new methodology, developed within the WP1 of the traceRadon project, to create low radon reference atmosphere of few Bq m^{-3} using low radon emanation sources developed by the alpha and gamma spectrometry group of the PTB (Röttger et al., 2023). The ARMON v2 was actually exposed within the climatic chamber of the PTB (see Appendix B, Fig. B1) under radon levels of few tens of Bq m^{-3} and during several months.

The PTB chamber has a nominal volume of $V = (21.035 \pm 0.030)$ m^3, which makes a calibration of larger devices inside the chamber possible. This chamber is equipped with a walkable air lock system and can be operated in a temperature range between -20 °C and +40 °C, as well as between 5 % to 95 % relative humidity. The pressure inside the chamber is recorded. The walls of the chamber consist of 100 mm polyurethane foam, clad inside and outside with stainless steel 0.6 mm in thickness. Due to this construction, the heat transmission coefficient is smaller than $k = 0.2$ W m^{-2} K^{-1}, which provides very stable calibration conditions. The inner wall is polished and connected to the ground, thus providing a homogeneous radon progeny field (Honig et al., 1998). Within the chamber the traceable [222]Rn activity concentration is established either via a [222]Rn gas standard (Dersch and Schötzig, 1998) or via primary [226]Ra emanation sources (Mertes et al., 2022). Due to the low activity concentrations values intended during this calibration (5 Bq m^{-3} to 20 Bq m^{-3}) the emanation source technique was used (Röttger et al., 2023). A [222]Rn free background was achieved, applying aged, synthetic, compressed air to the chamber, flushing all remainders of [222]Rn from it.

Extensive experiment over a period of 4 months with varying activity concentrations between (7.8 ± 0.4) Bq m^{-3} and (45.4 ± 0.8) Bq m^{-3} have been carried out. Even though dry air had been applied through the background determination, additional silica gel and a thoron delay volume were installed at the inlet of the ARMON v2, to prevent thoron progeny events and humidity during the experiment. All installations and detectors were completely installed inside the climate chamber, which was operated in a closed mode, to prevent any exchange with the surrounding low activity concentration lab air. All results are in consistence with this assumption.

3 Results and discussion

3.1 Theoretical efficiency

The EF and its force lines inside the sphere, when $V = 10$ kV was applied, was modelled with the COMSOL software, and are shown in Fig. 2a. The simulation of the tracks of 10000 randomly spaced particles in a 3D sphere using this EF (Fig.. 2b, 2c and 2d) shows that the 98 % of the $^{218}Po^+$ ions generated inside the spherical detection volume are collected inside the active area of the detector if we assume no interactions with other particles, decay, or neutralisation. Applying Eq. 4, and assuming that $p_{218_{Po^+}}$=0.88, p_{Active}= 0.98 and $p_{Detected}$=0.5, the maximum efficiency of our geometry, ε_g, in terms of counts detected per disintegrations inside the detection volume will be of 43 %. If we express the efficiency in terms of count rate (s^{-1}) per Bq m^{-3}, assuming a detection volume of 0.02 m^{-3}, the ε_g efficiency of our system is 0.0086 (Bq m^{-3})$^{-1}$ s^{-1}.

From the simulation of the trajectories of the 10000 polonium ions, the estimated travelling time of the particles to reach the detector surface will vary between 0 s and 1.8 10^{-2} s, depending on its distance from the detector, with a mean value of 8.9 10^{-3} s. During these travelling times, the probability of ^{218}Po decay events will be completely negligible, while the effect of the recombination with OH^- ions will cause a loss of particles from 0 % to 25 % in an interval between 0 ppmv and 2000 ppmv. Consequently, the collection efficiency ε_c will vary between 100 % at 0 ppmv and 75 % at 2000 ppmv, being 87.6 % at the nominal humidity of 400 ppmv.

Multiplying both geometrical and collection efficiencies, the maximum theoretical efficiency of our system, when no water is present, will be $\varepsilon_0 = 0.0086$ (Bq m^{-3})$^{-1}$ s^{-1}, while when working at 400 ppmv and 2000 ppmv of H_2O the theoretical ε will be 0.0075 (Bq m^{-3})$^{-1}$ s^{-1} and 0.0065 (Bq m^{-3})$^{-1}$ s^{-1} respectively. Fig. 3 shows the relationship between the estimated theoretical detection efficiency of the ARMON v2 in relation to the water content of the sampled air (blue line).

It should be take into account that during the simulations some hypothesis were done which may be not be entirely correct: i) no other recombination processes of the ^{218}Po ions were considered; ii) a regular spherical potential surface was considered to generate an EF with spherical symmetry although the real EF is expected to have some irregularities due to the inhomogeneous distribution of the potential over the sphere wall due, among others, to the presence of inlet and outlet tubbing connections; iii) no air diffusion effects were considered, iv) it has been observed in the results of the COMSOL simulations that a small vertical shift in the detector position could change the percent of particles collected on the active area of the detector surface. All these previous observations lead to the conclusion that the theoretical efficiency obtained for the ARMON v2 has only to be considered as the ideal highest value and not treated as nominal efficiency of the instrument.
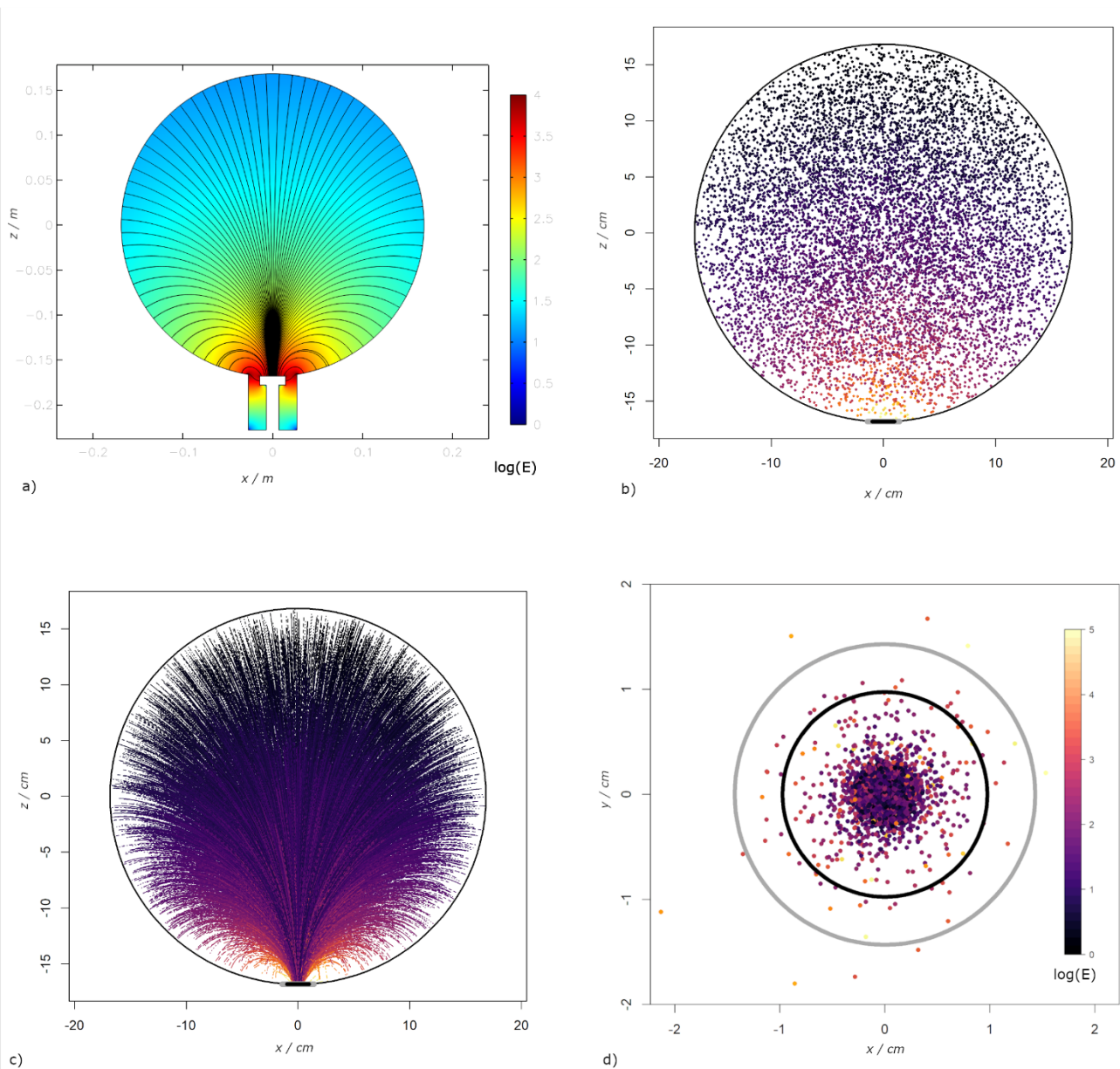
Figure 2. a): Simulation of the electrostatic field generated within the ARMON v2 detection volume with the application of 10 kV voltage, black lines represent the EF direction; b): Initial position inside the detection volume of the simulated ^{218}Po ions (10^5 fictitious particles); c): Trajectories of the simulated particles inside the sphere when the 10 kV voltage is applied between the sphere walls and the PIPS detector; d): Distribution of the simulated deposition of the charged ions at the detector surface. The inner black circle denotes the active area. The colour scale for Fig. 2b, 2c and 2d is the natural logarithm of the EF, in log(V/cm), and it is shown in Fig. 2d.

3.2 INTE Calibration results

Figure 3 shows the results of the water correction experiments carried out at the INTE-UPC and PTB chambers. A linear relationship between the detection efficiency of the instrument and the water vapour concentration is observed within a range of 150 ppmv - 2000 ppmv. This relationship was found to be independent on the radon concentration in a range of 600 Bq m^{-3} - 5900 Bq m^{-3}. When the water vapour concentration of the sampled air is above 2000 ppmv the relation loses this linearity and for this reason it is worth not to measure over this vapour concentration. In the range 150 ppmv - 2000 ppmv, the detection efficiency of the ARMON v2 may be corrected using Eq. 2 with b being equal to 5.4 10^{-7} (Bq m^{-3})$^{-1}$ s^{-1} ppmv^{-1} with an uncertainty (RSE) of 7.3 10^{-8} (Bq m^{-3})$^{-1}$ s^{-1} ppmv^{-1}.

Due to the increment observed in the detection efficiency for values of water vapour concentration lower than 150 ppmv, an exponential correction fit was also applied to the data following Eq. 13.

$$\varepsilon = \varepsilon_0' e^{(b'\,[H_2O]^{1/2})} \qquad (13)$$

The exponential curve (green dashed line) is also represented in Fig. 3 and may be more appropriate for very low water concentrations which are usually uncommon for sampled air at atmospheric stations. For this reason, the use of the linear fit is here proposed.
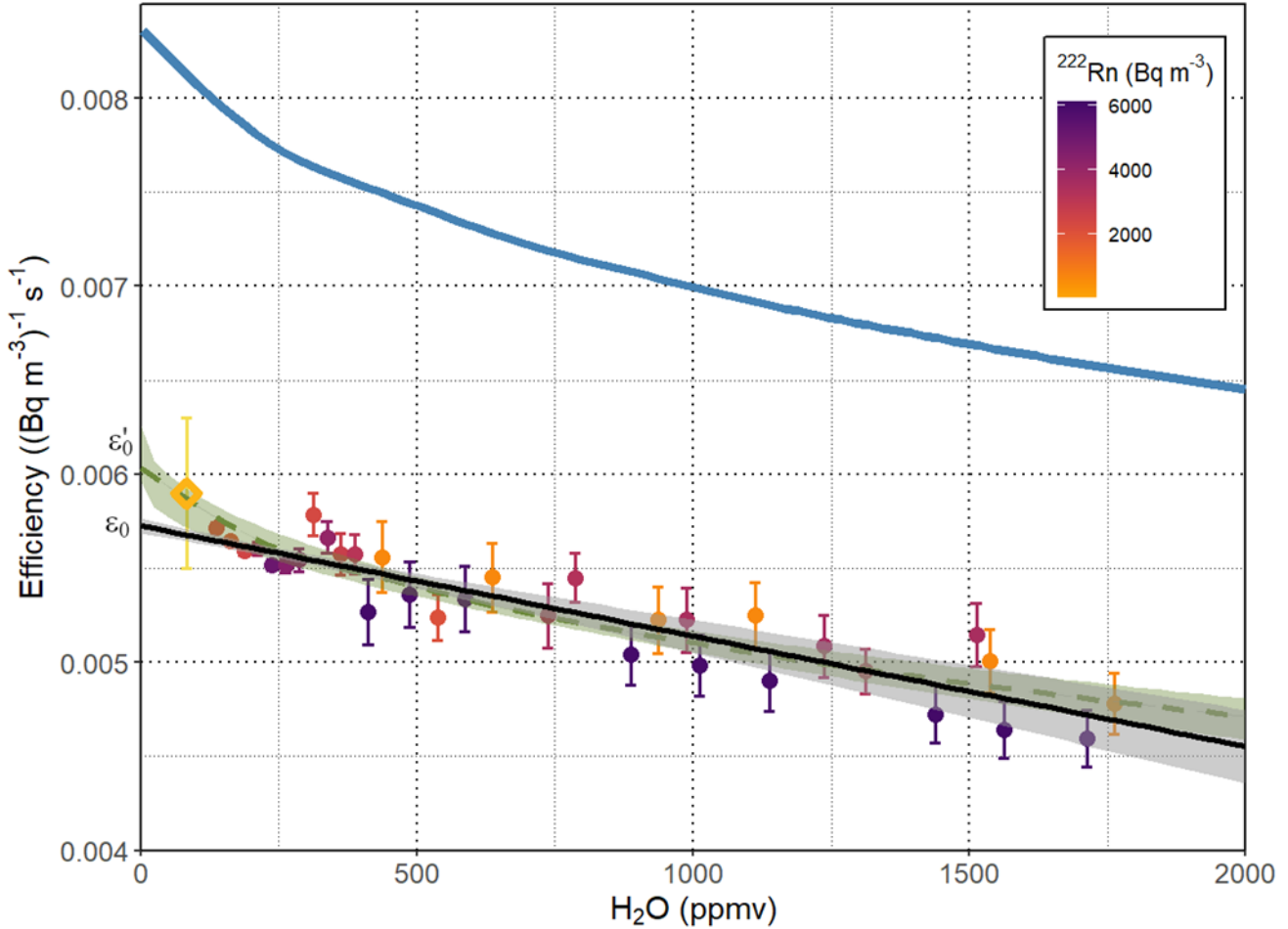
Figure 3: Dependence of the efficiency of the ARMON v2 monitor on to the water vapour concentration (in ppmv H₂O) at the detection volume. The coloured points are efficiency averages and its uncertainty in intervals of 10 ppmv of H₂O, of the efficiency of the hourly measurements for all the calibrations at INTE-UPC. The black line is the linear fit of the observational points with the 95 % confidence interval represented by the grey shaded zone. The green dotted curve is the exponential fit of the observational points with the 95 % confidence interval represented by the green shaded zone. The rhombus represents the efficiency of the ARMON at PTB with its uncertainty. The blue curve represents the theoretical efficiency simulation assuming a mobility of 3 cm² (V s)⁻¹. ε_0 is the y-interception of the linear fit e and ε_0' is the y-interception o the exponential fit.

Once determined the water correction coefficient b, the efficiency of the monitor ε_0 was calculated within the radon concentration range of 500 Bq m⁻³ - 6000 Bq m⁻³. From the results obtained (Fig. 4), a high linearity ($r^2 = 0.999$) in the regression between ²¹⁸Po counts against ²²²Rn concentration measured with the ATMOS monitor was observed. Within the calibration range (300 Bq m⁻³ - 6200 Bq m⁻³), and taking in consideration the ATMOS uncertainty, the ε_0 of the ARMON v2 calculated with the ATMOS monitor at the INTE chamber was of (0.0057 ± 0.0002) (Bq m⁻³) s⁻¹. If an exponential fit had been applied, the value of ε_0' obtained would have been (0.0061 ± 0.0002) (Bq m⁻³) s⁻¹.
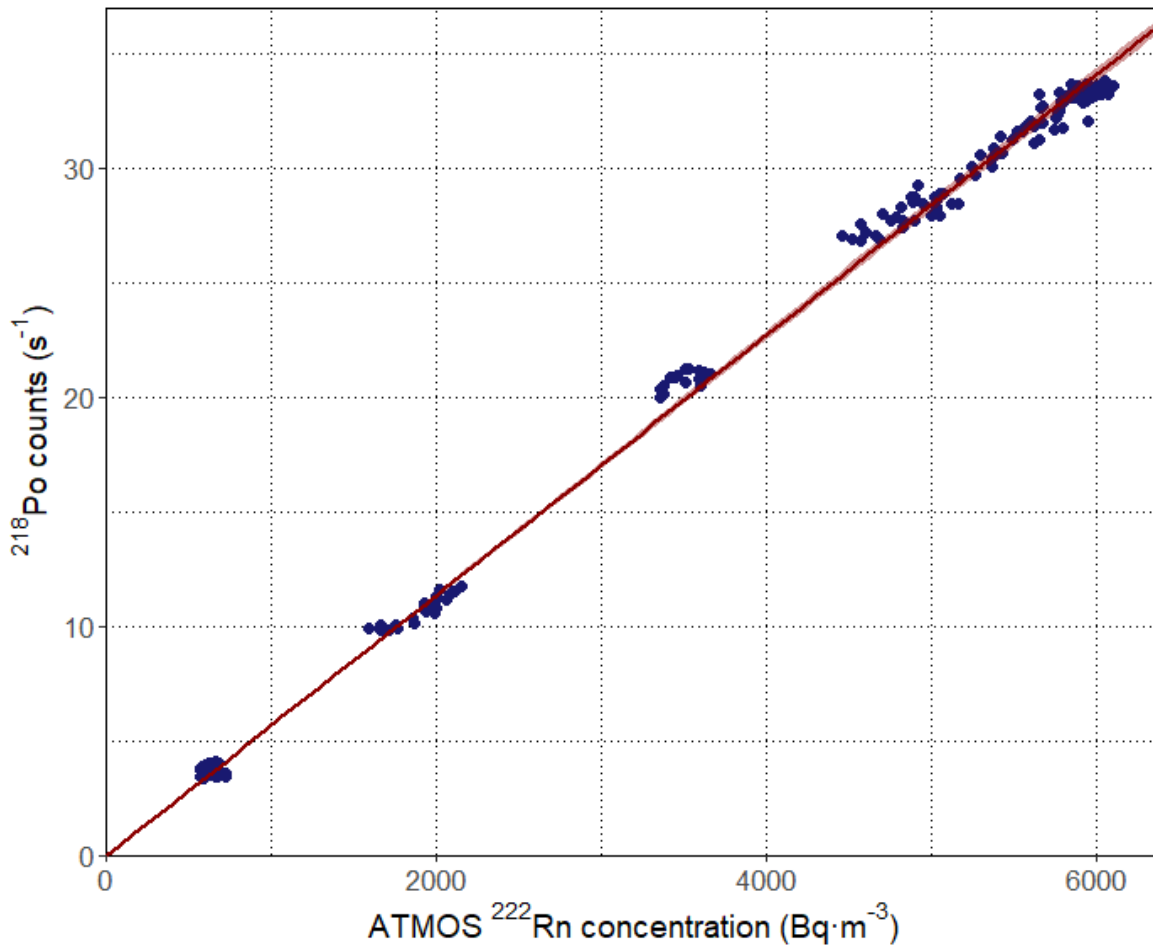
Figure 4: Calibration of the efficiency of the ARMON v2 monitor (^{218}Po counts against ^{222}Rn concentration) within the range 0 Bq m^{-3} – 6000 Bq m^{-3}.^{222}Rn concentration measured with an ATMOS monitor at the INTE-UPC radon chamber (hourly means). ^{218}Po counts (s^{-1}) from hourly spectra. Red line is the regression line (r^2 = 0.999).

It has to be underlined that the experimentally calculated efficiency of the ARMON v2 in the range between 300 ppmv - 2000 ppmv of $[H_2O]$ is 24 % lower than the theoretical one (assuming a mobility of 3 cm^2 (V s^{-1}). Although in the same order of magnitude, this difference could be explained, as described in Section 3.1, by a multitude of variables which could cause the ^{218}Po ions not to be collected at the detector surface.

3.3 Uncertainty, background and typical limits

The total uncertainty of the radon measurements performed with the ARMON v2 is calculated with Eq. 9. As example here it has been estimated for a typical atmospheric hourly radon measurement performed at the SAC atmospheric site (C_{Rn} = 4 Bq m^{-3}, T = 298 K, P = 1000 hPa, $[H_2O]$ = 250 ppmv and nc_{Po212} = 1). The uncertainty values for all parameters and its sensitivity coefficients are shown in Table 2. The combined uncertainty obtained was 0.46 Bq m^{-3}, which amount to 11 % of the absolute value of the measurement. The most influencing contribution in the calculation of the total uncertainty of the measurement is the uncertainty of the total net ^{218}Po counts, followed by the uncertainty of the detection efficiency and the uncertainty of the water vapour correction factor. As for the STP correction, the values of T and P uncertainties have been taken from the sensor uncertainties. A higher uncertainty could be due to the distance between the sensors positon and the detection volume of the instrument. However, calculus show that these uncertainties will be negligible. Let the Reader consider that an increase of the temperature uncertainty of 2 degrees will suppose an increase in the uncertainty of 1.4·10^{-3} Bq m^{-3}, and an increase of 5 hPa in the uncertainty of Pressure will only increase total uncertainty by 4·10^{-3} Bq m^{-3}.

410   Calculating the variability for a range of humidity (0 ppmv - 2000 ppmv), the total uncertainty of the measure has been plotted as a function of radon concentration (Fig. 5a). In the range of 0 ppmv – 400 ppmv, the total uncertainty is below the 10 % for radon concentrations greater than 5 Bq m^{-3}. For humidity greater than 1000 ppmv, the uncertainty increases due to the decrease of the detection efficiency.

Quantity	Estimate	Type	Standard uncertainty	Probability distribution	v_i	Sensitivity coefficient	Contribution to the standard uncertainty
X_i	x_i		$u(x_i)$			c_i	$u_i(y)$
nc_{Po218}	81	A	9	Normal	∞	0.0496	0.4466
nc_{Po212}	1	A	1	Normal	∞	−0.0279	-0.0279
ε_0	0.00575 (Bq m^{-3})$^{-1}$ s^{-1}	B	$1.7 \cdot 10^{-4}$	Normal	∞	−11.671	-0.1225
b	$5.4\ 10^{-7}$ (Bq m^{-3})$^{-1}$ s^{-1} ppmv^{-1}	B	$7.3\ 10^{-8}$	Normal	∞	2917.7	0.0117
$[H_2O]$	~250 ppmv	B	51	Normal	∞	$3.73\ 10^{-4}$	0.0190
P	~1000 hPa	B	0.3	Normal	∞	$−4.00\ 10^{-3}$	-0.0012
T	~298 K	B	0.746	Normal	∞	$1.1339\ 10^{-2}$	0.0100
C_{Rn}	4.0 Bq m^{-3}	Combined uncertainty (u) (Bq m^{-3})					0.47

415   **Table 2. Calculated contributions of the different variable and/or parameters to the total uncertainty of a typical radon concentration measurement performed with the ARMON v2 at an atmospheric station.**

In addition, given a typical water content in sampled air of 250 ppmv H$_2$O, the total uncertainty of the measurement has been also calculated taking into account different possible levels of thoron gas in the sample (Fig. 5b). It can be observed that when

420   the radon concentration increases to tens of Bq m^{-3}, the thoron concentration present in the sampled air has almost no effect on the uncertainty of the measurement. However, at low radon concentrations below 5 Bq m^{-3}, the thoron concentration can be an important source of uncertainty. This problem can be easily avoided using a thoron decay volume before the ARMON v2 detection volume. Within this scenario, the uncertainty at 0.6, 1, 2, 5, 10 and 100 Bq m^{-3} are of 29 %, 22 %, 16 %, 10 %, 7.7 % and 5.1 % respectively.

425   a)
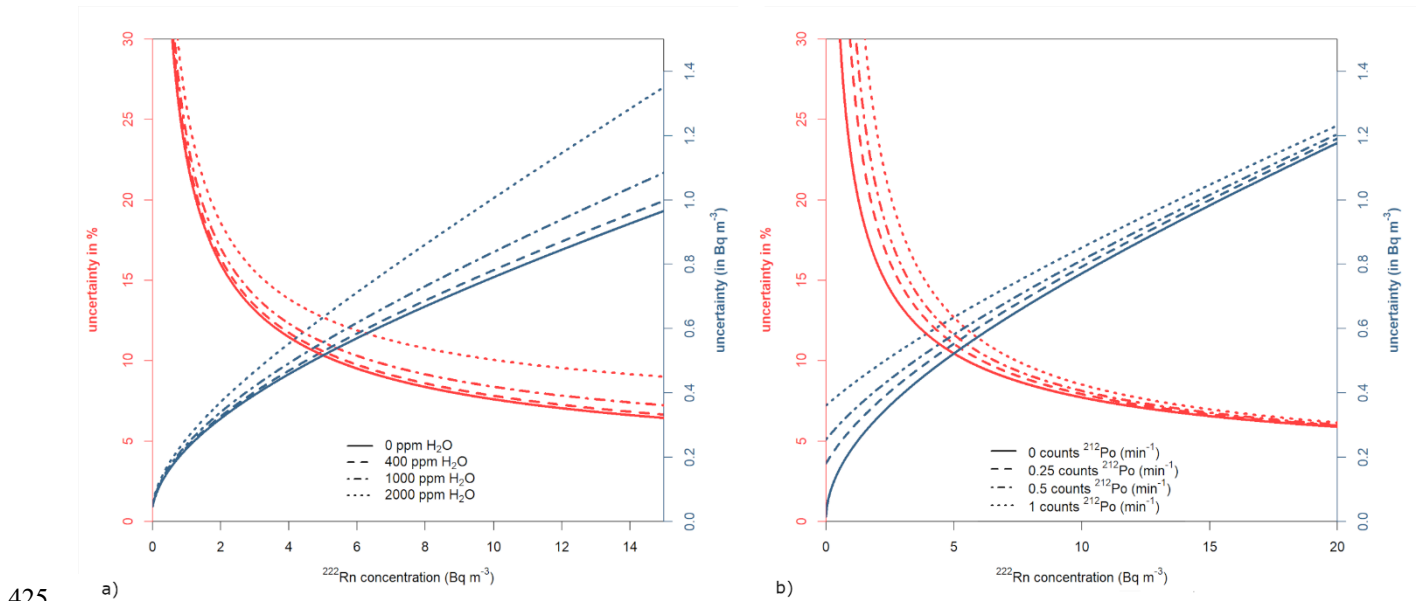
Figure 5: a): absolute (blue) and relative (red) uncertainty as a function of ^{222}Rn activity concentration at different water vapour concentrations. b): absolute (blue) and relative (red) uncertainty as a function of ^{222}Rn activity concentration at different ^{212}Po (thoron decay) concentrations.

430 As an additional information, it may be of interest to explain that during the INTE-UPC experiments it was discovered that the silica gel material may contain thorium material which is a thoron source. Actually, hourly spectra showed up to 1 count per minute (min^{-1}) of ^{212}Po, which means 0.56 min^{-1} of ^{212}Bi α-decays to ^{208}Tl and this implies an increase greater than 50 % of the uncertainty for radon concentrations below 5 Bq m^{-3}. For this reason, and although the content of thorium material within commercial silica gel has not yet been quantitatively estimated, authors highly recommend not to use this dryer for radon

435 measurements or using a delay volume of at least 10 L between the Silica Gel dryer and the selected radon instrument. Generally, authors suggest the use of other drying systems as Nafion tubes or cold traps.

In regard to the detection limit and the decision threshold of the ARMON v2, these previous values are only dependent on the presence of thoron concentrations within the detection volume. When no thoron counts are present (e.g. when using a buffer

440 volume before the ARMON v2), the decision threshold is 0.045 Bq m^{-3}, corresponding to 1 count per hour, and the detection limit is $a^{\#} = 0.132$ Bq m^{-3}, with an uncertainty of 0.08 Bq m^{-3}. At a typical thoron concentration at atmospheric sites (100 m tall towers) of 0.017 min^{-1}, the detection limit and the decision threshold are 0.3 Bq m^{-3} and 0.08 Bq m^{-3} respectively. The change of the characteristic limits as a function of the ^{212}Po detected count rate in min^{-1} is shown in Fig. 6.
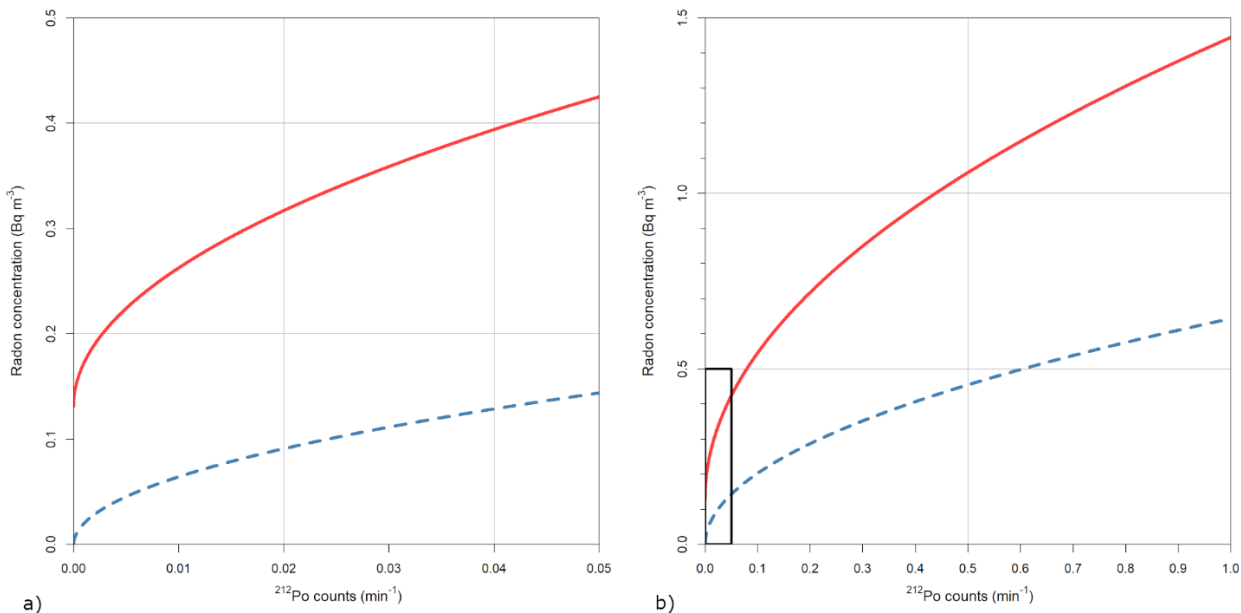
445

Figure 6: Radon activity concentration detection limit (red straight) and decision threshold (dashed blue) of the ARMON v2 monitor from a) 0 counts to 0.05 counts min^{-1} and b) 0 counts to 1 count min^{-1} of ^{212}Po detected.

3.4 PTB results

Figure 7 shows a summary of the results of the values of the detection efficiency of the ARMON v2 obtained by INTE-UPC

450 (orange dots) and PTB (blue dots) experiments. Both experiments, carried out under different conditions of radon concentrations, show a linearity in the counts detected by the instrument and the radon concentrations to be measured (Fig. 7a). Totally, five calibration points with three different emanation sources were realised at the PTB (see Appendix B Fig. B2).

During the ARMON v2 exposures at the PTB climate chamber, the sampled air had an average water content of 83 ± 21 ppmv

455 for the whole measurement campaign (Fig. 3, gold rhombus) and thus the estimated detection efficiency was corrected applying the exponential fit (Eq. 13).

Since five calibration points with three different emanation sources were realised (see Appendix B Fig. B2) and the characterisation of the sources had been done with the same instruments, the statistical correlation of the error distributions has to be further investigated in detail. A full correlation of the sources and their uncertainties was considered at this point, which probably overestimates the total uncertainty of the calibration and increases the uncertainty about a factor of two, with respect to just ignoring the correlation.

Taking all this into account, the sensitivity of the ARMON v2 (ε_0') that was determined during the calibration described in Section 2.5 was (0.0062 ± 0.0008) $(Bq\ m^{-3})^{-1}\ s^{-1}$. This result is in good agreement with the one obtained from INTE-UPC when the exponential fit is applied (0.0061 ± 0.0002), as previously reported in 3.2. The offset determined during this calibration is with $(0.002 \pm 0.007)\ s^{-1}$ in good agreement with the theoretical 0.

The detection efficiency of the ARMON v2, within its uncertainty, do not change when the radon concentrations vary between few Bq m^{-3} and thousands of Bq m^{-3} (Fig. 7b). This is an important output which confirms the robustness of this instrument and its response. This last result also allows to accept and to use the detection efficiency value obtained at high radon concentrations and for this reason with a much smaller uncertainty. Additionally, the stability of the linearity in time and in a wide range of radon concentrations of the detection efficiency of the ARMON v2, proves its suitability to be used as a transfer standard for in situ calibration and/or comparison of others radon and radon progeny monitors.

a)   b)
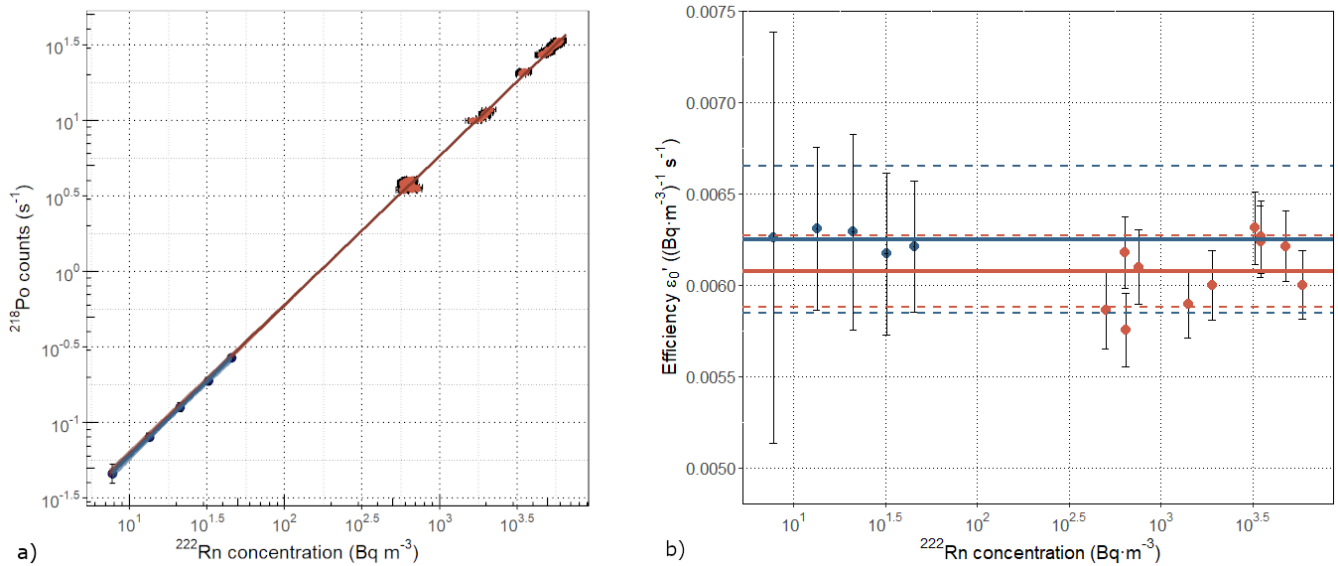
Figure 7: a) Counts per second versus radon concentration (dots) and regression lines for the detection efficiency obtained during INTE-UPC experiments (orange) and PTB experiments (blue), with the 99 % confidence level shadowed. b) Dots: detection efficiency (ε_0') of the ARMON v2 and its uncertainty versus radon concentration for the different exposures at PTB (blue) and INTE-UPC (orange). Solid lines are the mean of the efficiency values obtained at PTB (blue) and INTE (orange), with its uncertainty at $k=1$ (dashed lines). X axis for both figures and Y axis for Fig. 7a are in logarithmic scale.

If the linear correction was used for the water vapour conditions (Fig. 3), the detection efficiency ε_0 obtained at PTB experiments will be of (0.00595 ± 0.0008), also within the uncertainty range of the efficiency obtained during INTE calibrations (0.00575 ± 0.0002). Results of the calibration at PTB, done 18 months after the calibration at INTE, also confirm that the calibration of the instrument is stable over the time, as it was already appreciated in the older version of the monitor (Grossi et al., 2012, 2018; 2020; Vargas et al., 2015). However, in the mark of calibration procedures of radon measurement network it is suggested to perform periodical stability checks of the efficiency of the different radon and radon progeny instruments running at the different stations.

4 Summary, conclusions and further steps

In this paper, a new version of the Atmospheric Radon MONitor (ARMON) is described. This new version is more robust and transportable than the previous prototype, can be easily installed at atmospheric stations and can be remotely controlled thank to a GUI window.

For the first time ever, the response of the ARMON v2 has been fully characterized by both theoretical and experimental approaches to obtain its detection efficiency for different radon concentrations, spanning between few Bq m^{-3} and thousands of Bqm^{-3}. A total uncertainty budget of the ARMON v2 monitor has been also carried out for the first time. Independent experiments were carried out both at the INTE-UPC radon chamber and at the PTB climate chamber in the framework of the European project traceRadon.

The monitor detection efficiency was found to be (0.0057 ± 0.0002) (Bq m^{-3})$^{-1}$ s^{-1} according to the INTE-UPC exposures results, and of (0.00595 ± 0.0008) (Bq m^{-3})$^{-1}$ s^{-1} according to the PTB experiments. The combined uncertainty of the ARMON v2 is lower than 10 % for radon activity values higher than 5 Bq m^{-3} and the detection limit 0.132 Bq m^{-3} when no thoron concentration is present in the sampled air. The theoretical detection efficiency was of $(0.0075$ (Bq m^{-3})$^{-1}$ s$^{-1})$, which is a 27 % higher than the real one, assuming that there are factors that where not taken into account as possible irregularities of the Electrostatic Field or recombination od ^{218}Po^{+} ions with other particles.

The linearity of the ARMON v2 response observed thanks to the INTE-UPC and PTB experiments allows the instrument to be calibrated at high concentration values and thus to reduce the calibration uncertainty.

In addition to the present full characterization of the ARMON v2, another completely different calibration method based on short pulse of ^{222}Rn was applied at PTB in the framework of the same traceRadon project. Due to the special features of the ARMON v2 detector, this will allow for very short calibration or recalibration, also outside a calibration chamber and under field conditions. Results are still under investigation and will be the object of a future paper. Finally, the ARMON v2 was also compared under field conditions with the new ANSTO 200 L (Chambers et al., 2022) and its results will be published in a third scientific paper.

From the results of the present study, it can be confirmed that the ARMON v2 can be considered a good transfer standard for in situ calibration of radon and radon progeny monitors installed at atmospheric sites according to the requirements of the atmospheric radon community.

Appendix A. ARMON v2 supplementary figures
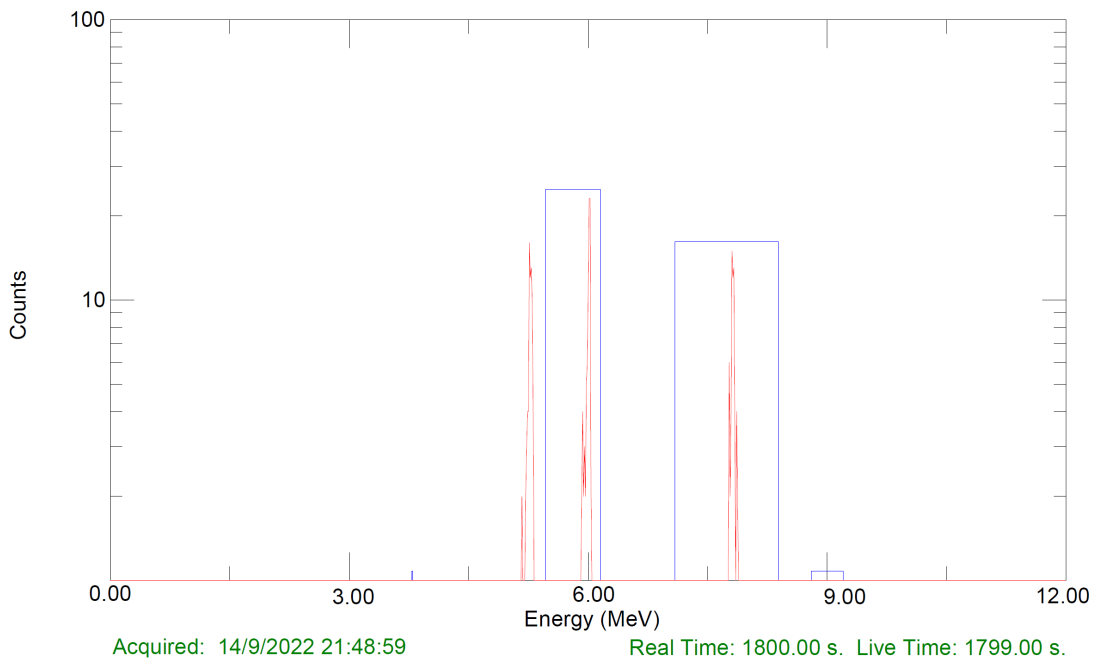
Figure A1: Typical spectrum from the ARMON v2 monitor with the ²¹⁰Po (5.30 MeV), ²¹⁸Po (6.0 MeV) and ²¹⁴Po (7.69 MeV) peaks observed. No ²¹²Po and ²¹⁴Po counts are observed.
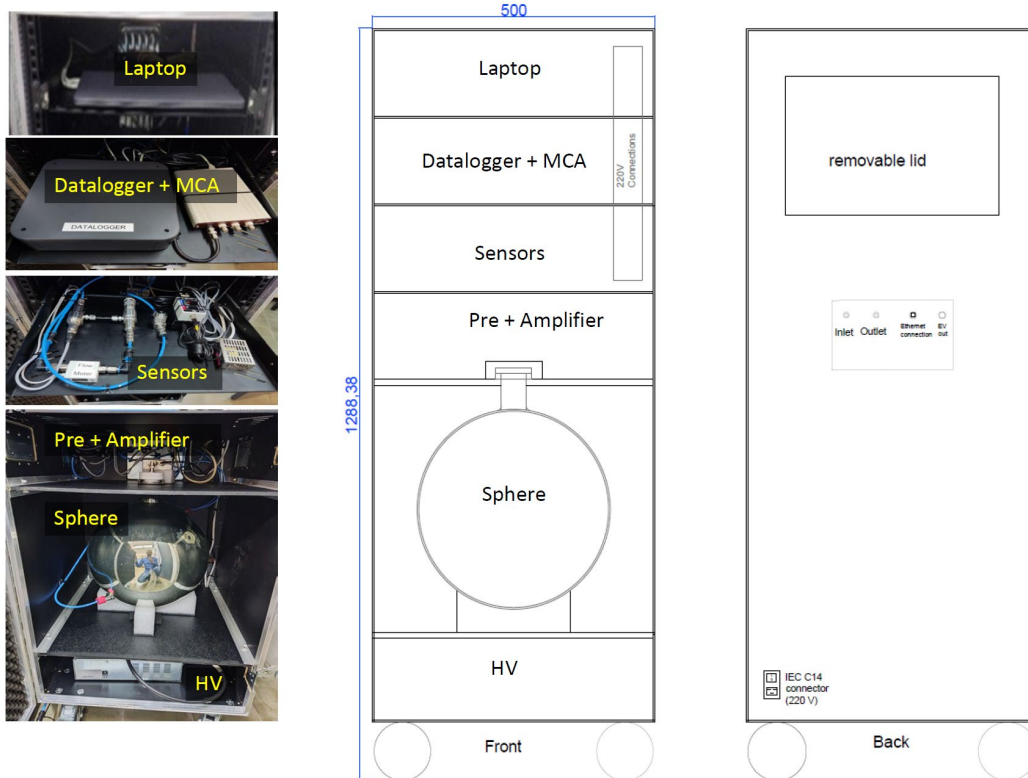
525

Figure A2: ARMON v2 monitor. Left: Trays and parts. Middle and *r*ight: inside and back drawing.
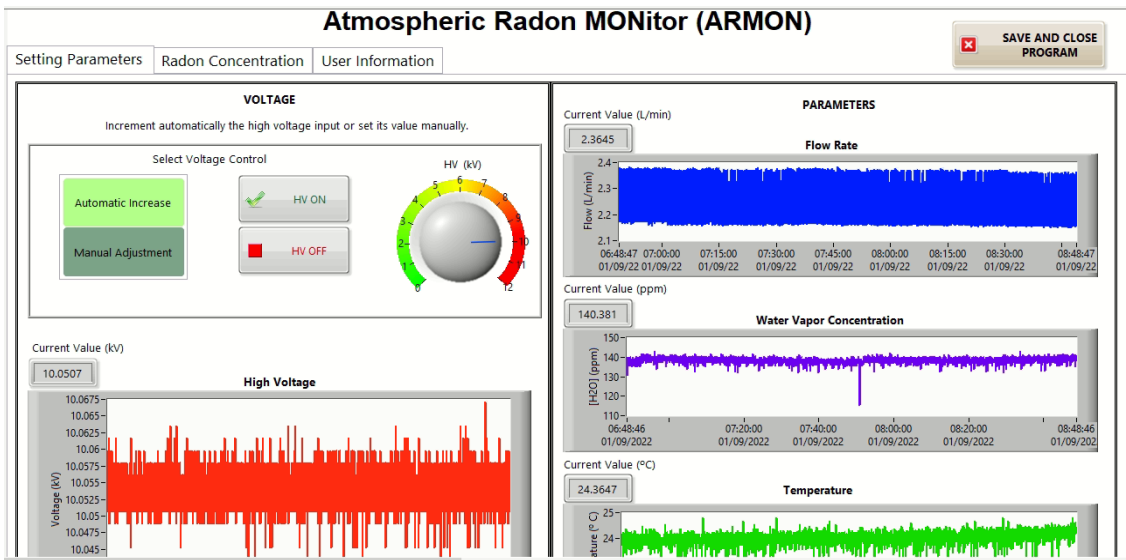
530 a)
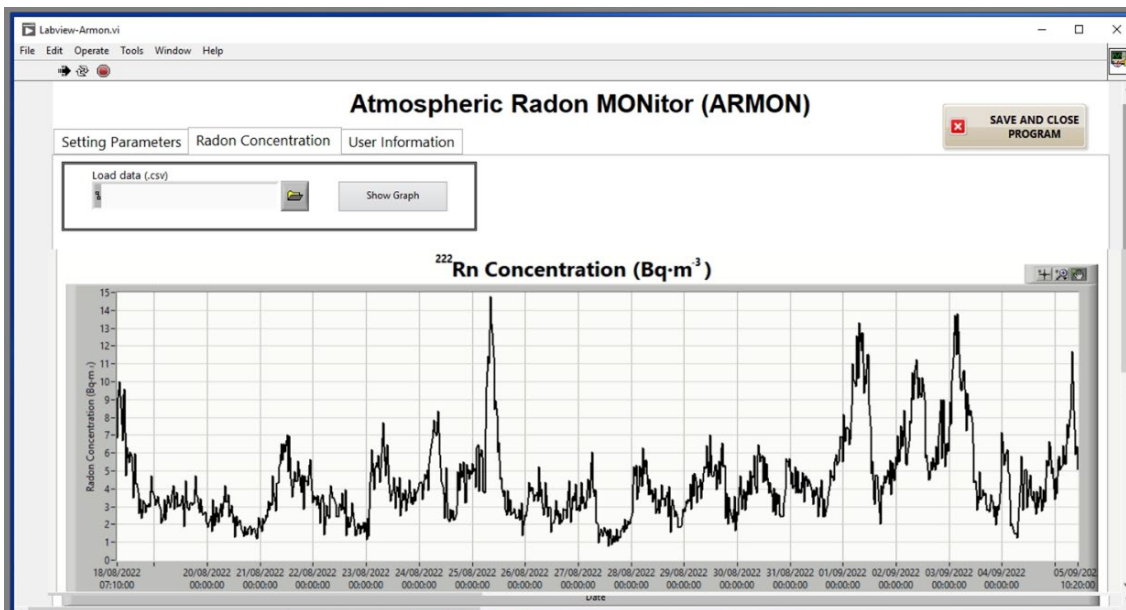
b)

Figure A3: User interface of the new ARMON v2 monitor. a) Sensor and voltage control b) Radon concentration visualization tab.

535
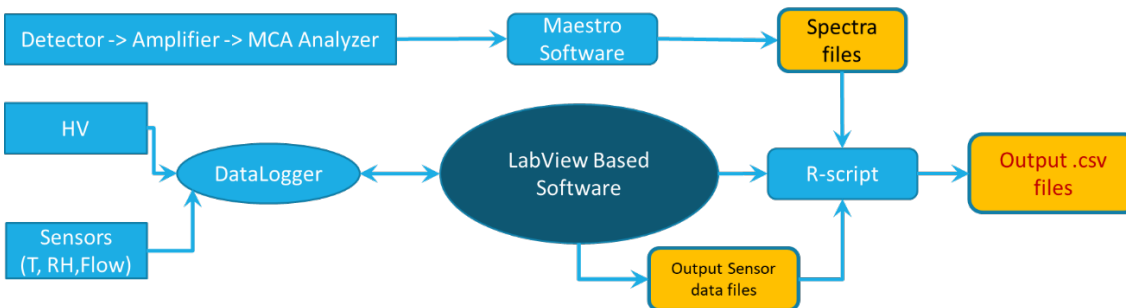
Figure A4: Data flow chart of the ARMON v2.

Appendix B. Calibration at PTB climatic chamber supplementary figures
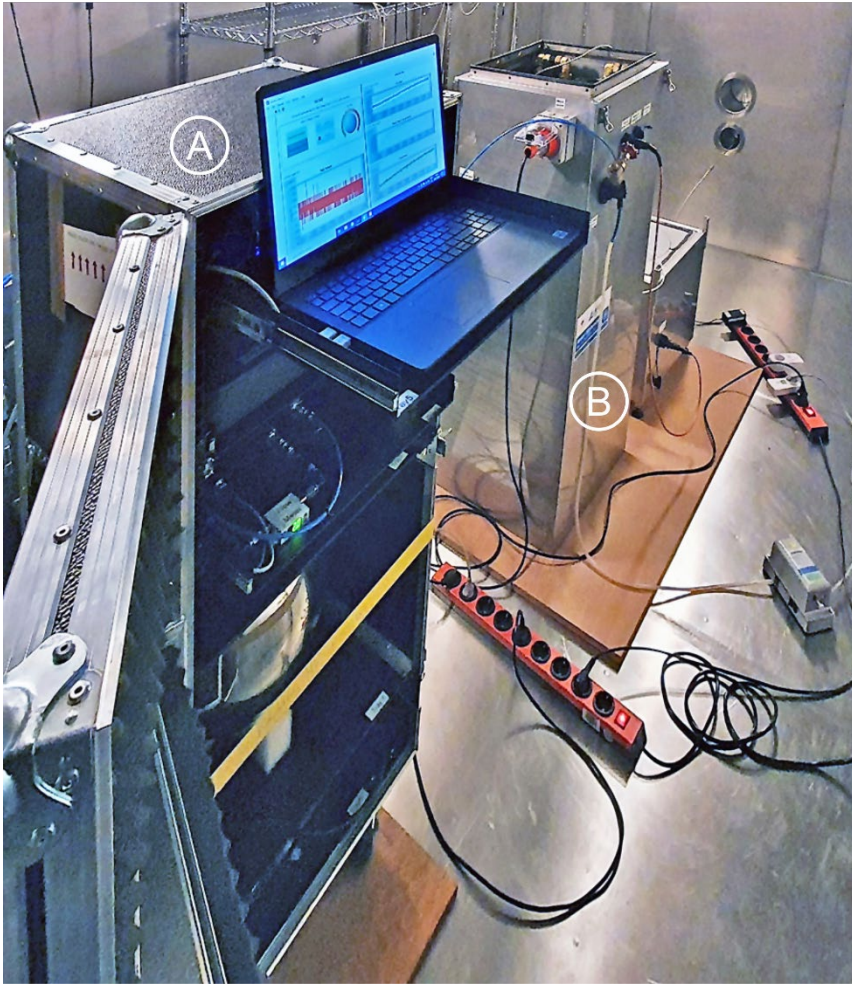
540

Figure B1: Picture of the calibration setup of the ARMON v2 in the calibration chamber at PTB. In the foreground you see the opened case of the ARMON v2 (A) and in the background a monitoring system developed by ANSTO (B) (Chambers et al., 2022).
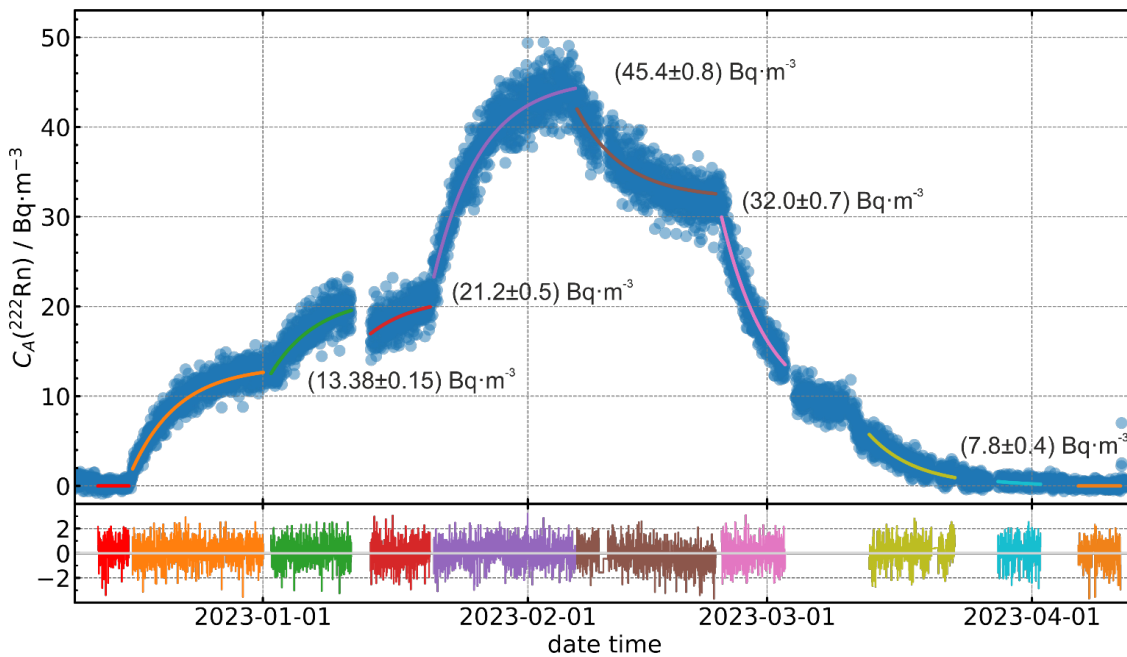
545 **Figure B2: Radon activity concentration determined with the ARMON v2 using three different emanation sources in five combinations. The values given in the figure illustrate the equilibrium activity concentration reached after infinite time with this source combination. The blue dots show the measured results of the ARMON v2 acquired during 30 min per point. The coloured**

lines show the modelled activity concentration determined from the emanation sources combination. The respective coloured lines in the lower graph show the relative residual between model and measurement, which proofs the excellent agreement.

550

Appendix C. drying unit

The drying system used with the ARMON v.2 is based on two steps drying: a Peltier cooler and drying through two silica gel cylinders. This system is capable of drying the air up to a water concentration between 150 ppm and 300 ppm.

In the first step, the Peltier cools down the inlet air to a 2 °C temperature and extracts the condensed water. Then a 3-way valve

555 allows redirecting the flow to each of the two silica gel cylinders that capture water molecules of air. After the silica cylinders, a retention valve before a T connection assures a unidirectional flow. After that, a 7 microns filter avoids silica dust to get over the circuit.

As the silica gel can release small quantities of ^{220}Rn, a 10 L tank is used to prevent thoron entries into the detection volume. After the 10 L buffer, the air can be introduced into the ARMON v2.

560 Figure C1 shows the basic scheme of the drying system. Two photographs of the drying unit are shown in Fig. C2.
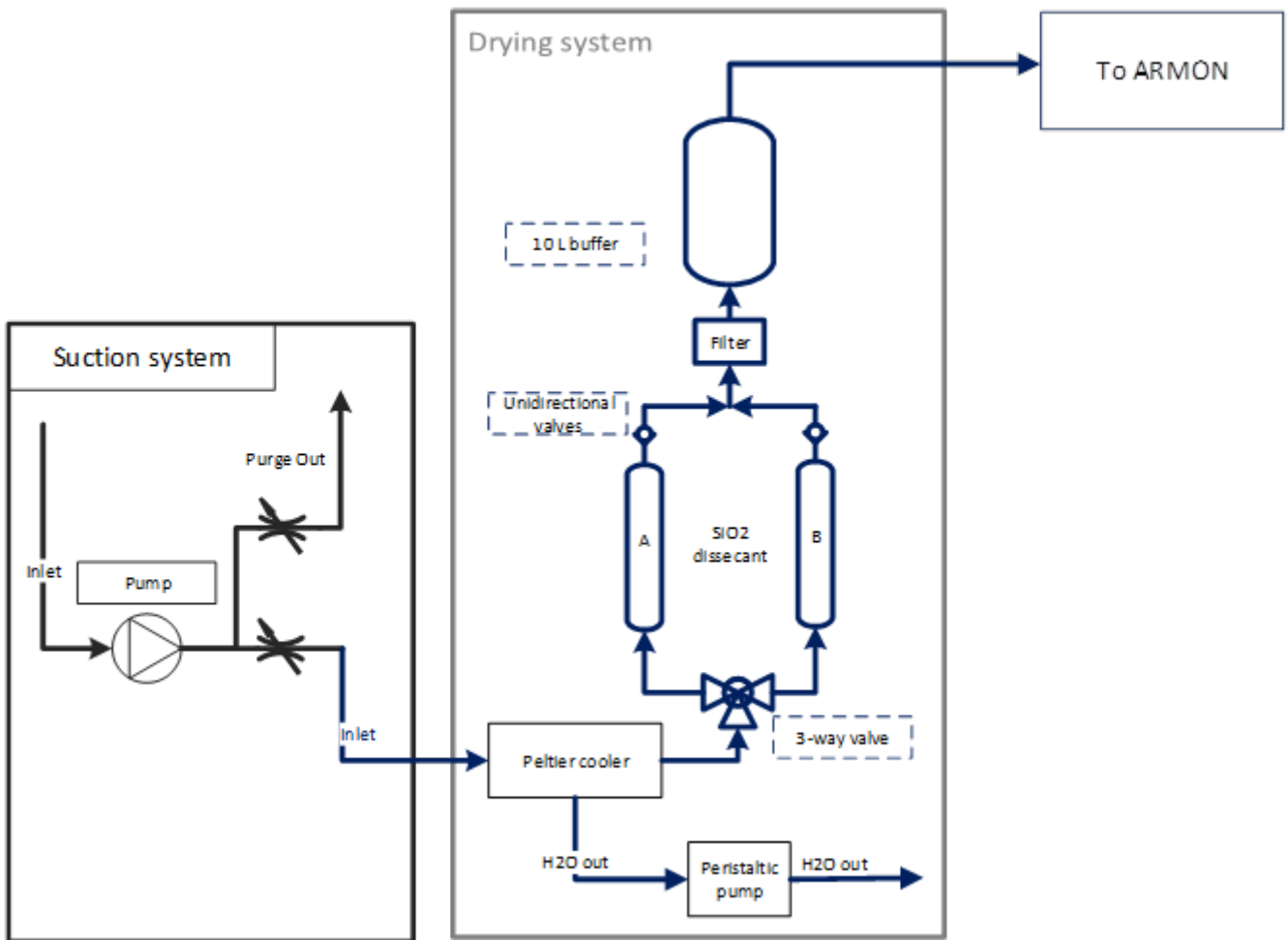
Figure C.1: Basic scheme of the INTE-UPC drying system.

565
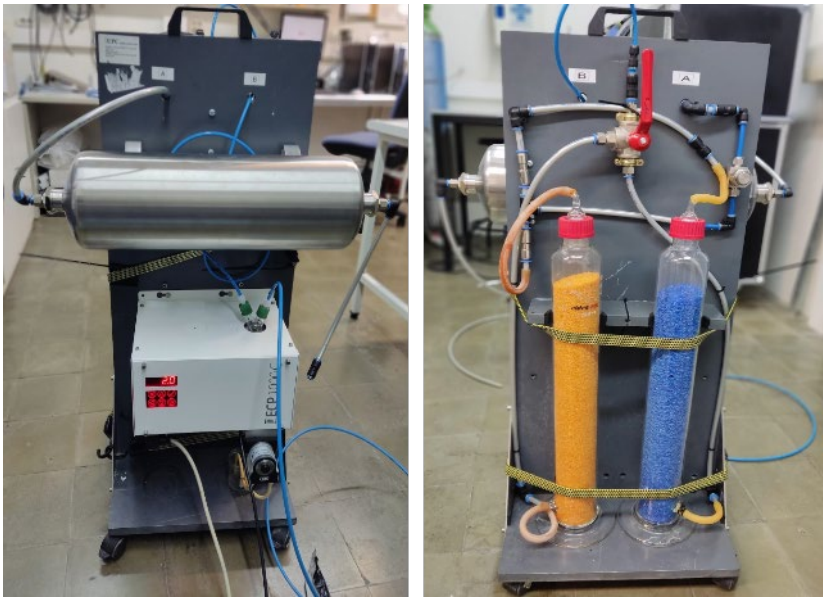
Figure C.2.: Front and back of the drying unit.

Code availability

The data and codes for this paper are available at the CORA Repositori de Dades de Recerca with doi
https://doi.org/10.34810/data893,

Data availability

The data and codes for this paper are available at the CORA Repositori de Dades de Recerca with doi
https://doi.org/10.34810/data893,

Author contributions

RC in the framework of his PhD project built the new version of the ARMON, ran the calibration experiments at the INTE-UPC and analysed the data with their corresponding uncertainties. RG and CG designed the COMSOL setting simulations for the theoretical efficiency analysis. AV and CG supervised the work as PI and co-PIs of the MAREA project and senior researchers of the traceRadon project. SR carried out the ARMON v2 exposures at the PTB and the related data analysis. RC led the manuscript writing and all authors contribute to it. All authors have read and agreed to the published version of the paper.

Competing interests

The authors declare that they have no conflict of interests.

Acknowledgments

The authors want to acknowledge Annette Röttger as coordinator of the traceRadon project for her work and continuous support. The authors also want to acknowledge Liza Shiro for her work in the developing of the ARMON-Labview program, Juan Antonio Romero for his support during the ARMON v2 building, Anja Honig and Tanita Ballé for their support during the ARMON v2 exposures at the PTB and Florian Mertes for his interesting ideas during the development of the low radon emanation sources of the PTB.

590 **Financial support**

This project was financed by the MAR2EA (IU68-017047) project and the 19ENV01 traceRadon project, which has received funding from the EMPIR programme co-financed by the Participating States and from the European Union's Horizon 2020 research and innovation programme.

References

595 Arnold, D., Vargas, A., Vermeulen, A. T., Verheggen, B. and Seibert, P.: Analysis of radon origin by backward atmospheric transport modelling, Atmos. Environ., 44(4), 494–502, doi:10.1016/j.atmosenv.2009.11.003, 2010.

Baskaran, M.: Po-210 and Pb-210 as atmospheric tracers and global atmospheric Pb-210 fallout: a Review, J. Environ. Radioact., 102(5), 500–513, doi:10.1016/j.jenvrad.2010.10.007, 2011.

Baskaran, M.: Radon: A Tracer for Geological, Geophysical and Geochemical Studies, Springer International Publishing,
600 Cham., 2016.

BIPM, IEC, IFCC, ILAC, ISO, IUPAC, IUPAP and OIML: Evaluation of measurement data - Guide to the expression of uncertainty in measurement, [online] Available from: https://www.bipm.org/documents/20126/2071204/JCGM%5C_100%5C_2008%5C_E.pdf/cb0ef43f-baa5-11cf-3f85-4dcd86f77bd6, 2008.

605 Chambers, S., Williams, A. G., Zahorowski, W., Griffiths, A. and Crawford, J.: Separating remote fetch and local mixing influences on vertical radon measurements in the lower atmosphere, Tellus, Ser. B Chem. Phys. Meteorol., 63(5), 843–859, doi:10.1111/j.1600-0889.2011.00565.x, 2011.

Chambers, S., Williams, A., Griffiths, A., Podstawczyńska, A., Pawlak, W. and Fortuniak, K.: Characterizing the State of the Urban Surface Layer Using Radon-222, J. Geophys. Res., 124(2), doi:10.1029/2018JD029507, 2019.

610 Chambers, S. D., Williams, A. G., Conen, F., Griffiths, A. D., Reimann, S., Steinbacher, M., Krummel, P. B., Steele, L. P., van der Schoot, M. V., Galbally, I. E., Molloy, S. B. and Barnes, J. E.: Towards a universal "Baseline" characterisation of air masses for high- and low-altitude observing stations using radon-222, Aerosol Air Qual. Res., 16(3), 885–899, doi:10.4209/aaqr.2015.06.0391, 2016.

Chambers, S. D., Griffiths, A. D., Williams, A. G., Sisoutham, O., Morosh, V., Röttger, S., Mertes, F. and Röttger, A.: Portable
615 two-filter dual-flow-loop 222Rn detector: stand-alone monitor and calibration transfer device, Adv. Geosci., 57, 63–80, doi:10.5194/adgeo-57-63-2022, 2022.

COMSOL: Documentation for comsol release 5.1, COMSOL Multiphysics, Inc., MA, 2015.

Conen, F. and Robertson, L. B.: Latitudinal distribution of radon-222 flux from continents, Tellus B Chem. Phys. Meteorol., 54(2), 127–133, doi:10.3402/tellusb.v54i2.16653, 2002.

620 Dankelmann, V., Reineking, A. and Postend rfer, J.: Determination of Neutralisation Rates of 218Po Ions in Air, Radiat. Prot. Dosimetry, 94(4), 353–357, doi:10.1093/oxfordjournals.rpd.a006510, 2001.

Dersch, R. and Schötzig, U.: Production and measurement of 222Rn standards, Appl. Radiat. Isot., 49(9–11), 1171–1174, doi:10.1016/S0969-8043(97)10040-9, 1998.

Galmarini, S.: One year of222Rn concentration in the atmospheric surface layer, Atmos. Chem. Phys., 6(10), 2865–2887,
625 doi:10.5194/acp-6-2865-2006, 2006.

Goldstein, S. D. and Hopke, P. K.: Environmental Neutralization of Polonium-218, Environ. Sci. Technol., 19(2), 146–150, doi:10.1021/es00132a006, 1985.

Grossi, C.: 222Rn as a tracer for air mass transport characterization at 100-m-high tower in the south-west Spanish coast. [online] Available from: http://www.tdx.cat/handle/10803/125236, 2012.

630 Grossi, C., Arnold, D., Adame, J. A., López-Coto, I., Bolívar, J. P., De La Morena, B. A. and Vargas, A.: Atmospheric 222Rn

concentration and source term at El Arenosillo 100 m meteorological tower in southwest Spain, Radiat. Meas., 47(2), 149–162, doi:10.1016/j.radmeas.2011.11.006, 2012.

Grossi, C., Àgueda, A., Vogel, F. R., Vargas, A., Zimnoch, M., Wach, P., Martín, J. E., López-Coto, I., Bolívar, J. P., Morguí, J. A. and Rodó, X.: Analysis of ground-based 222Rn measurements over Spain: Filling the gap in southwestern Europe, J.

635   Geophys. Res. Atmos., 121(18), 11,021-11,037, doi:10.1002/2016JD025196, 2016.

Grossi, C., Vogel, F. R., Curcoll, R., Àgueda, A., Vargas, A., Rodó, X., Morguí, J.-A., Grossi, C., Vogel, F. R. and By, C. C.: Study of the daily and seasonal atmospheric CH4 mixing ratio variability in a rural Spanish region using 222Rn tracer, Atmos. Chem. Phys., 18(8), 5847–5860, doi:10.5194/acp-18-5847-2018, 2018.

Grossi, C., Chambers, S. D., Llido, O., Vogel, F. R., Kazan, V., Capuana, A., Werczynski, S., Curcoll, R., Delmotte, M.,

640   Vargas, A., Morguí, J.-A., Levin, I. and Ramonet, M.: Intercomparison study of atmospheric 222Rn and 222Rn progeny monitors, Atmos. Meas. Tech., 13(5), 2241–2255, doi:10.5194/amt-13-2241-2020, 2020.

Gutiérrez-Álvarez, I., Guerrero, J. L., Martín, J. E., Adame, J. A., Vargas, A. and Bolívar, J. P.: Radon behavior investigation based on cluster analysis and atmospheric modelling, Atmos. Environ., 201(December 2018), 50–61, doi:10.1016/j.atmosenv.2018.12.010, 2019.

645   Hernández-Ceballos, M. A., Vargas, A., Arnold, D. and Bolívar, J. P.: The role of mesoscale meteorology in modulating the 222Rn concentrations in Huelva (Spain) - impact of phosphogypsum piles, J. Environ. Radioact., 145, 1–9, doi:10.1016/j.jenvrad.2015.03.023, 2015.

Hirao, S., Yamazawa, H. and Moriizumi, J.: Estimation of the Global 222Rn Flux Density from the Earth's Surface, Japanese J. Heal. Phys., 45(2), 161–171, doi:10.5453/jhps.45.161, 2010.

650   Honig, A., Paul, A., Röttger, S. and Keyser, U.: Environmental control of the German radon reference chamber, Nucl. Instruments Methods Phys. Res. Sect. A Accel. Spectrometers, Detect. Assoc. Equip., 416(2–3), 525–530, doi:10.1016/S0168-9002(98)00788-8, 1998.

Hopke, P. K.: Use of Electrostatic Collection of 218Po for Measuring Rn, Health Phys., 57(1), 39–42, doi:10.1097/00004032-198907000-00005, 1989.

655   ICOS RI: ICOS Atmosphere Station Specifications V2.0 (editor: O. Laurent)., 2020.

Jacob, D. J. and Prather, M. J.: Radon-222 as a test of convective transport in a general circulation model, Tellus B, 42(1), 118–134, doi:10.1034/j.1600-0889.1990.00012.x, 1990.

Karstens, U., Schwingshackl, C., Schmithüsen, D. and Levin, I.: A process-based 222radon flux map for Europe and its comparison to long-term observations, Atmos. Chem. Phys., 15(22), 12845–12865, doi:10.5194/acp-15-12845-2015, 2015.

660   Levin, I., Glatzel-Mattheier, H., Marik, T., Cuntz, M., Schmidt, M. and Worthy, D. E.: Verification of German methane emission inventories and their recent changes based on atmospheric observations, J. Geophys. Res. Atmos., 104(D3), 3447–3456, doi:10.1029/1998JD100064, 1999.

Levin, I., Born, M., Cuntz, M., Langendörfer, U., Mantsch, S., Naegler, T., Schmidt, M., Varlagin, A., Verclas, S. and Wagenbach, D.: Observations of atmospheric variability and soil exhalation rate of radon-222 at a Russian forest site.

665   Technical approach and deployment for boundary layer studies, Tellus B Chem. Phys. Meteorol., 54(5), 462–475, doi:10.3402/tellusb.v54i5.16681, 2002.

Levin, I., Karstens, U., Hammer, S., DellaColetta, J., Maier, F. and Gachkivskyi, M.: Limitations of the Radon Tracer Method (RTM) to estimate regional Greenhouse Gases (GHG) emissions – a case study for methane in Heidelberg, Atmos. Chem. Phys., 21(23), 1–34, doi:10.5194/acp-21-17907-2021, 2021.

670   Mertes, F., Röttger, S. and Röttger, A.: Development of 222Rn Emanation Sources with Integrated Quasi 2π Active Monitoring, Int. J. Environ. Res. Public Health, 19(2), 840, doi:10.3390/ijerph19020840, 2022.

Nazaroff, W. and Nero, A. V: Radon and its decay products in indoor air, John Wiley and Sons Inc, New York, NY (USA)., 1988.

ORTEC: MAESTRO v7.0 User's Manual, [online] Available from: https://www.ortec-online.com/-/media/ametekortec/manuals/a/a65-mnl.pdf?la=en&revision=f2f3ed3f-fa2d-4185-9301-7d480b0a6955, 2012.

Pal, S., Lopez, M., Schmidt, M., Ramonet, M., Gibert, F., Xueref-Remy, I. and Ciais, P.: Investigation of the atmospheric boundary layer depth variability and its impact on the 222 Rn concentration at a rural site in France, J. Geophys. Res. Atmos., 120(2), 623–643, doi:10.1002/2014JD022322, 2015.

Pugliese, M., Baiano, G., Boiano, A., D'Onofrio, A., Roca, V., Sabbarese, C. and Vollaro, P.: A compact multiparameter acquisition system for radon concentration studies, Appl. Radiat. Isot., 53(1–2), 365–370, doi:10.1016/S0969-8043(00)00154-8, 2000.

Radulescu, I., Calin, M. R., Luca, A., Röttger, A., Grossi, C., Done, L. and Ioan, M. R.: Inter-comparison of commercial continuous radon monitors responses, Nucl. Instruments Methods Phys. Res. Sect. A Accel. Spectrometers, Detect. Assoc. Equip., 1021(October 2021), 165927, doi:10.1016/j.nima.2021.165927, 2022.

Röttger, A., Röttger, S., Grossi, C., Vargas, A., Curcoll, R., Otáhal, P., Hernández-Ceballos, M. Á., Cinelli, G., Chambers, S., Barbosa, S. A., Ioan, M., Radulescu, I., Kikaj, D., Chung, E., Arnold, T., Yver-Kwok, C., Fuente, M., Mertes, F. and Morosh, V.: New metrology for radon at the environmental level, Meas. Sci. Technol., 32(12), 124008, doi:10.1088/1361-6501/ac298d, 2021.

Röttger, S., Röttger, A., Mertes, F., Morosch, V., Ballé, T. and Chambers, S.: Evolution of traceable radon emanation sources from MBq to few Bq, Appl. Radiat. Isot., 196(February), doi:10.1016/j.apradiso.2023.110726, 2023.

Schery, S. D. and Huang, S.: An estimate of the global distribution of radon emissions from the ocean, Geophys. Res. Lett., 31(19), 1–4, doi:10.1029/2004GL021051, 2004.

Schmidt, M., Graul, R., Sartorius, H. and Levin, I.: Carbon dioxide and methane in continental Europe: a climatology, and 222 Radon-based emission estimates, Tellus B Chem. Phys. Meteorol., 48(4), 457–473, doi:10.3402/tellusb.v48i4.15926, 1996.

Schmithüsen, D., Chambers, S., Fischer, B., Gilge, S., Hatakka, J., Kazan, V., Neubert, R., Paatero, J., Ramonet, M., Schlosser, C., Schmid, S., Vermeulen, A., Levin, I., Attribution, C. C., Schmith, D. and Levin, I.: A European-wide 222radon and 222radon progeny comparison study, Atmos. Meas. Tech., 10(4), 1299–1312, doi:10.5194/amt-10-1299-2017, 2017.

Szegvary, T., Conen, F. and Ciais, P.: European 222Rn inventory for applied atmospheric studies, Atmos. Environ., 43(8), 1536–1539, doi:10.1016/j.atmosenv.2008.11.025, 2009.

Tositti, L., Pereira, E. B., Sandrini, S., Capra, D., Tubertini, O. and Bettoli, M. G.: Assessment of Summer Trends of Tropospheric Radon Isotopes in a Coastal Antarctic Station (Terra Nova Bay), Int. J. Environ. Anal. Chem., 82(5), 259–274, doi:10.1080/03067310290027767, 2002.

Vargas, A., Ortega, X. and Martín Matarranz, J. .: Traceability of radon-222 activity concentration in the radon chamber at the technical university of Catalonia (Spain), Nucl. Instruments Methods Phys. Res. Sect. A Accel. Spectrometers, Detect. Assoc. Equip., 526(3), 501–509, doi:10.1016/j.nima.2004.02.022, 2004.

Vargas, A., Arnold, D., Adame, J. A., Grossi, C., Hernández-Ceballos, M. A. and Bolivar, J. P.: Analysis of the vertical radon structure at the spanish "El arenosillo" tower station, J. Environ. Radioact., 139, 1–17, doi:10.1016/j.jenvrad.2014.09.018, 2015.

Vogel, F. R., Ishizawa, M., Chan, E., Chan, D., Hammer, S., Levin, I. and Worthy, D. E. J.: Regional non-CO2 greenhouse gas fluxes inferred from atmospheric measurements in Ontario, Canada, J. Integr. Environ. Sci., 9(sup1), 41–55, doi:10.1080/1943815X.2012.691884, 2012.

Wada, A., Matsueda, H., Murayama, S., Taguchi, S., Hirao, S., Yamazawa, H., Moriizumi, J., Tsuboi, K., Niwa, Y. and Sawa, Y.: Quantification of emission estimates of CO2, CH4 and CO for east asia derived from atmospheric radon-222 measurements over the western North Pacific, Tellus, Ser. B Chem. Phys. Meteorol., 65(1), 1–16, doi:10.3402/tellusb.v65i0.18037, 2013.

WADA, A., MURAYAMA, S., KONDO, H., MATSUEDA, H., SAWA, Y. and TSUBOI, K.: Development of a Compact and Sensitive Electrostatic Radon-222 Measuring System for Use in Atmospheric Observation, J. Meteorol. Soc. Japan. Ser. II,

88(2), 123–134, doi:10.2151/jmsj.2010-202, 2010.

Whittlestone, S. and Zahorowski, W.: Baseline radon detectors for shipboard use: Development and deployment in the First Aerosol Characterization Experiment (ACE 1), J. Geophys. Res. Atmos., 103(D13), 16743–16751, doi:10.1029/98JD00687, 1998.

Williams, A. G., Chambers, S. D., Conen, F., Reimann, S., Hill, M., Griffiths, A. D. and Crawford, J.: Radon as a tracer of atmospheric influences on traffic-related air pollution in a small inland city, Tellus, Ser. B Chem. Phys. Meteorol., 68(1), doi:10.3402/tellusb.v68.30967, 2016.

Zahorowski, W., Chambers, S. D. and Henderson-Sellers, A.: Ground based radon-222 observations and their application to atmospheric studies, J. Environ. Radioact., 76(1–2), 3–33, doi:10.1016/j.jenvrad.2004.03.033, 2004.